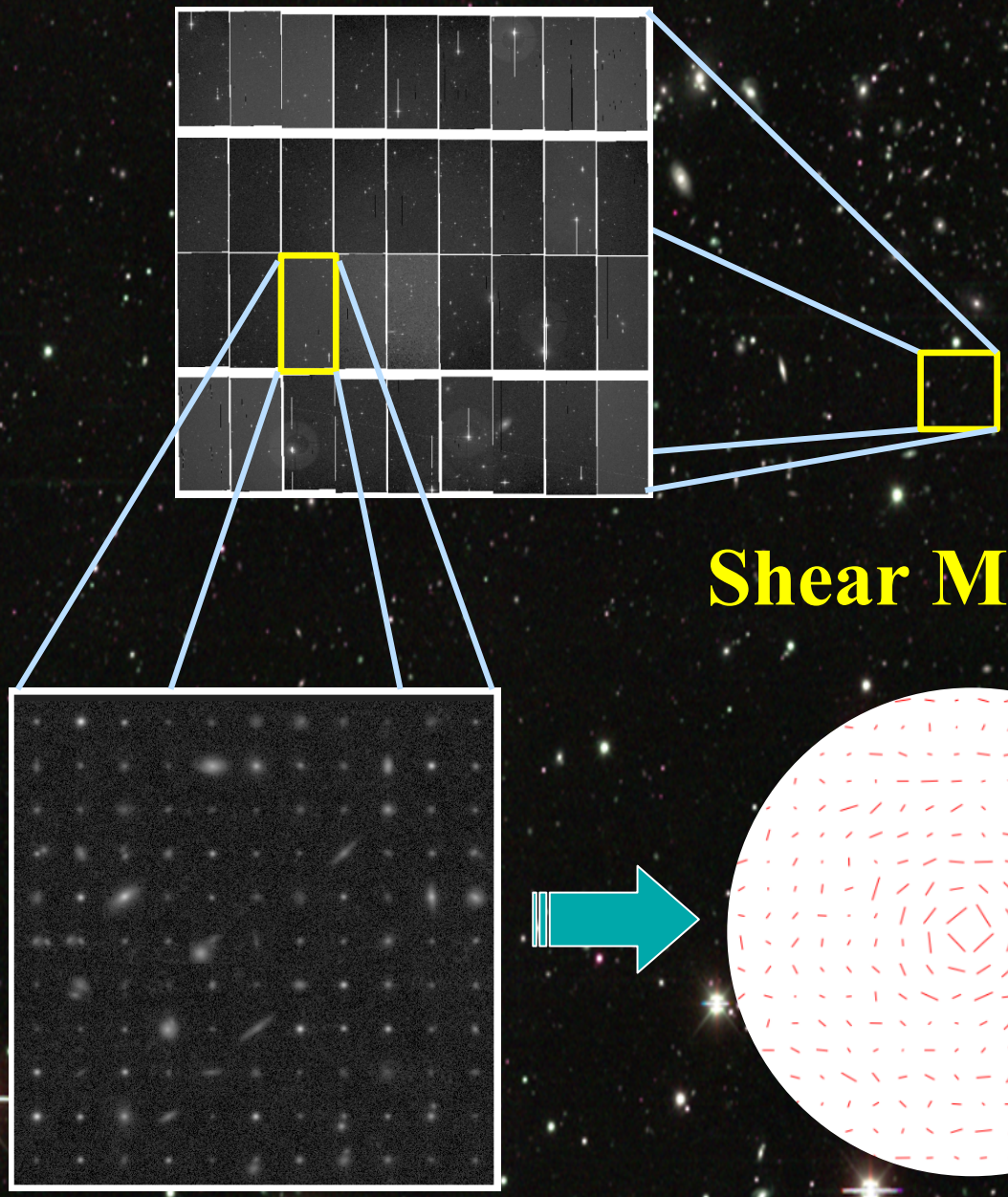

Shear Measurement -- CSST Progresses & Concerns

Jun Zhang
Shanghai Jiao Tong University

ISSI -BJ Meeting, Beijing, Nov 4 - Nov 8, 2019

Outline:

- Progresses
- Concerns

Outline:

- Progresses
- Concerns

Our Opportunities & Challenges

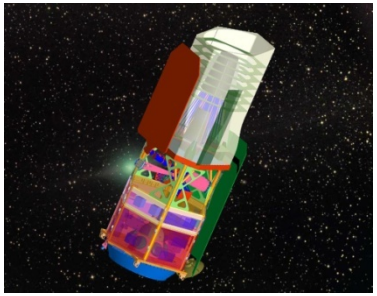

WFIRST

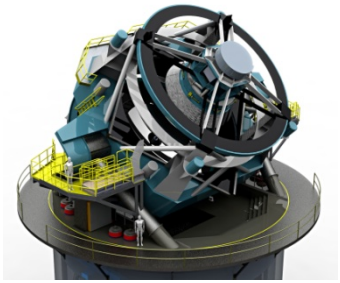

LSST

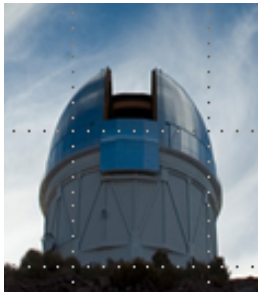

DES

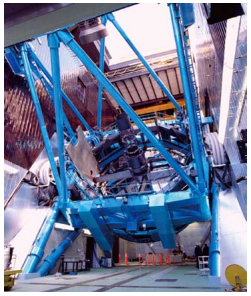

Subaru HSC

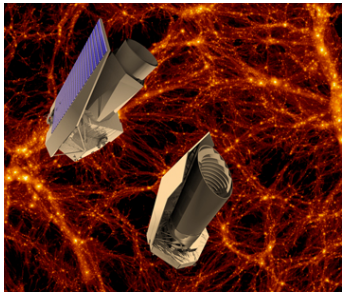

EUCLID

CSST(CHINA)

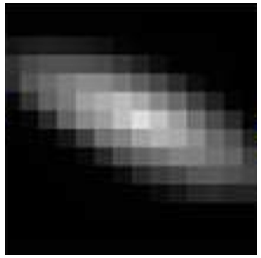

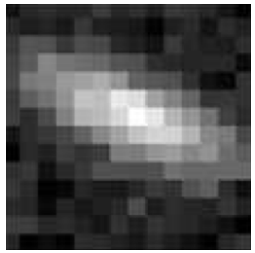

Project Name	HSC	DES	LSST	Euclid	WFIRST	CSS-OS
Starting Time	2014	2013	2022	2020	2025	~2022
Survey Area	1400deg^2	5000deg^2	18000deg^2	15000deg^2	2700deg^2	17500deg^2
Galaxy Number	~ 0.1B	~0.3B	~ 2B	~ 1B	~0.3B	~ 1B

Opportunities & Challenges

Lensing is Low: Cosmology, Galaxy Formation, or New Physics?

Alexie Leauthaud[1,2], Shun Saito[3], Stefan Hilbert[4,5], Alexandre Barreira[3], Sur
Martin White[6], Shadab Alam[7,8], Peter Behroozi[6,9], Kevin Bundy[1,2], Jean Cou
Thomas Erben[11], Catherine Heymans[8], Hendrik Hildebrandt[11], Rachel Mand
Lance Miller[12], Bruno Moraes[13], Maria E. S. Pereira[14], Sergio A. Rodríguez-T
Fabian Schmidt[3], Huan-Yuan Shan[18], Matteo Viel[19,20], Francisco Villaescusa-
[1]*Department of Astronomy and Astrophysics, University of California, Santa Cruz, 1156 High Street, Santa Cruz, CA 95064*
[2]*Kavli IPMU (WPI), UTIAS, The University of Tokyo, Kashiwa, Chiba, 277-8583, Japan*
[3]*Max-Planck-Institut für Astrophysik, Karl-Schwarzschild-Starße 1, D-85740 Garching bei München, Germany*
[4]*Exzellenzcluster Universe, Boltzmannstr. 2, 85748 Garching, Germany*
[5]*Ludwig-Maximilians-Universität, Universitäts-Sternwarte, Scheinerstr. 1, 81679 München, Germany*
[6]*Department of Physics, University of California, Berkeley, CA 94720*
[7]*McWilliams Center for Cosmology, Department of Physics, Carnegie Mellon University, Pittsburgh, PA 15213*
[8]*The Scottish Universities Physics Alliance, Institute for Astronomy, University of Edinburgh, Blackford Hill, Edinburgh EH9 3HJ, UK*
[9]*H*

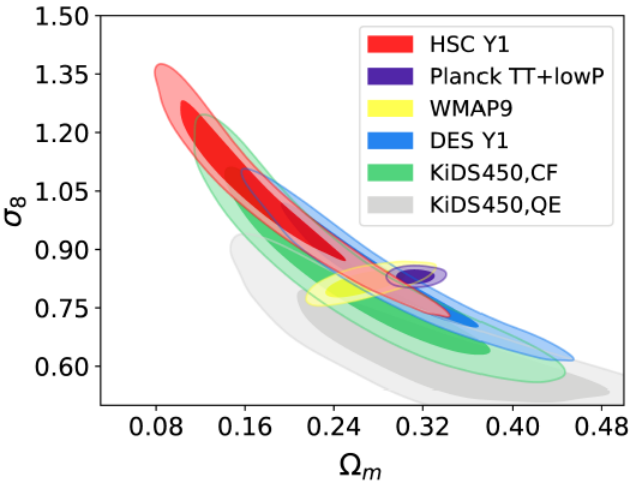

Problems with KiDS

George Efstathiou and Pablo Lemos
Kavli Institute for Cosmology Cambridge and Institute of Astronomy, Madingley Road, Cambridge, CB3 OHA.

4 July 2017

ABSTRACT
The Kilo-Degree Survey (KiDS) has been used in several recent papers straints on the amplitude of the matter power spectrum and matter redshift. Some of these analyses have claimed tension with the *Planc* mology at the $\sim 2-3\sigma$ level, perhaps indicative of new physics. Ho is consistent with other low redshift probes of the matter power spec redshift space distortions and the combined galaxy-mass and galaxy- spectra. Here we perform consistency tests of the KiDS data, finding int for various cuts of the data at $\gtrsim 3\sigma$ significance. Until these interna understood, we argue that it is premature to claim evidence for new KiDS.

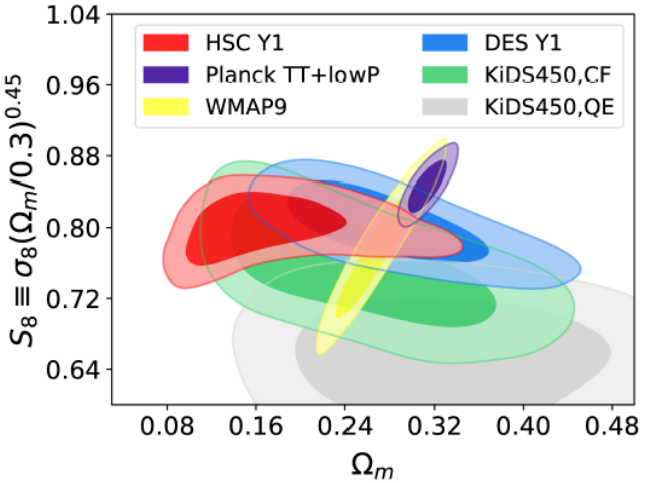

Chiaki Hikage et al.,
arXiv:1809.09148

KSB+ Method

$$Q_{ij}\left(x^O, y^O\right) = \frac{\int d^2\vec{\theta} \cdot W\left(\vec{\theta}\right) f^O\left(\vec{\theta}\right) \theta_i \theta_j}{\int d^2\vec{\theta} \cdot W\left(\vec{\theta}\right) f^O\left(\vec{\theta}\right)}$$

$$\begin{pmatrix} \varepsilon_1 \\ \varepsilon_2 \end{pmatrix} = \frac{1}{Q_{11} + Q_{22}} \begin{pmatrix} Q_{11} - Q_{22} \\ 2Q_{12} \end{pmatrix}$$

$$\Gamma_\alpha = \left(P^\gamma\right)^{-1}_{\alpha\beta} \left[\varepsilon_\beta - P^{sm}_{\beta\mu} p_\mu\right]$$

Heymans et al. (2006)

Shapelets Method

$$G_{model} = P \cdot \left(1 + \varepsilon_1 S_1 + \varepsilon_2 S_2\right) \cdot C$$

$$\gamma_i = \frac{\left\langle \varepsilon_i \right\rangle}{1 - \left\langle \varepsilon_1^2 + \varepsilon_2^2 \right\rangle}$$

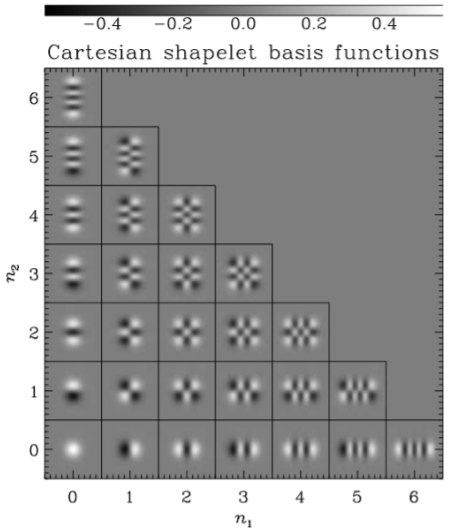

Kuijken (2006)

BJ02 Method

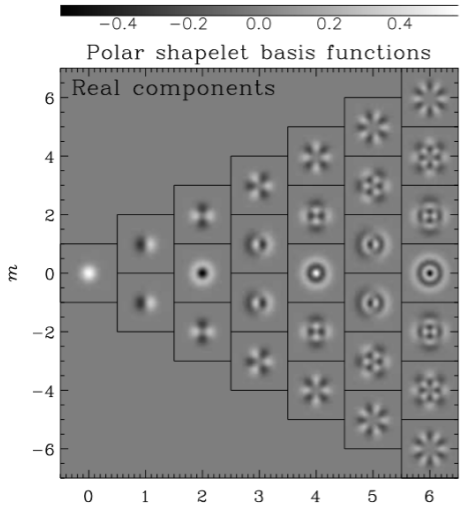

Bernstein & Jarvis (2002)

Bayesian Shape Measurement Method (Lensfit)

$$\chi^2 = \sum_i \left[\frac{y_i - SBg_i - S(1-B)f_i}{\sigma_i}\right]^2$$

Miller et al. (2013)

A Different Approach

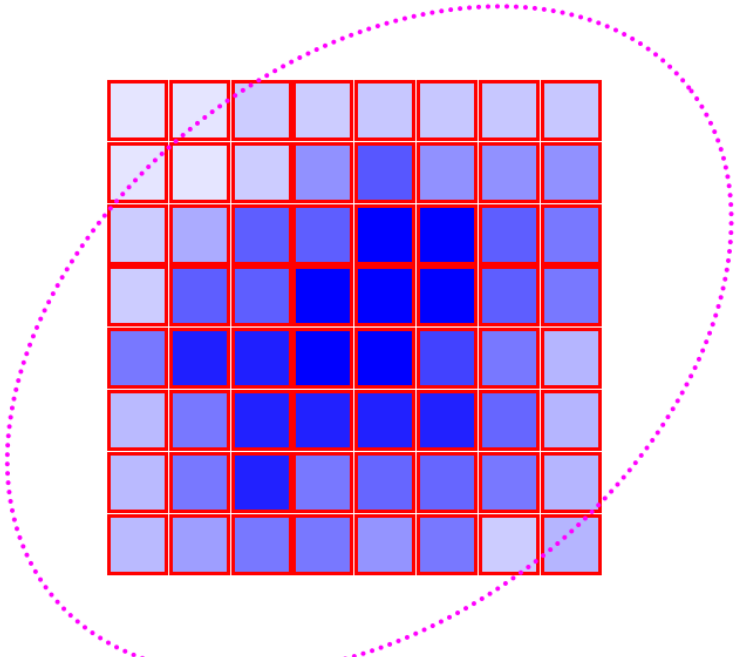

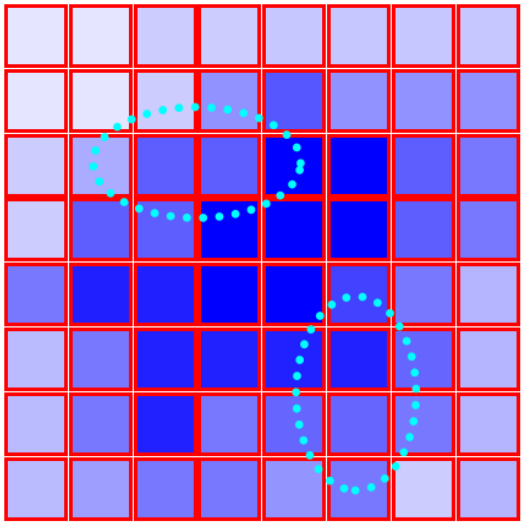

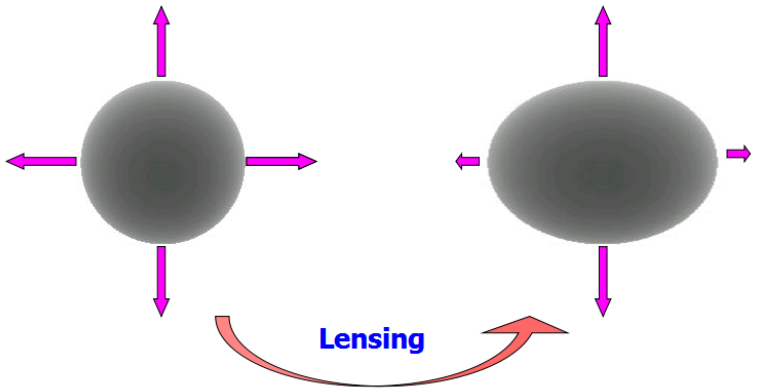

➢ **For perfect seeing condition:**

$$\gamma_1 = -\frac{1}{2}\frac{\langle (\partial_x f)^2 - (\partial_y f)^2 \rangle}{\langle (\partial_x f)^2 + (\partial_y f)^2 \rangle}$$

$$\gamma_2 = -\frac{\langle \partial_x f \partial_y f \rangle}{\langle (\partial_x f)^2 + (\partial_y f)^2 \rangle}$$

Seljak & Zaldarriaga, 1999

In the presence of an isotropic Gaussian PSF

$$\gamma_1 = -\frac{1}{2}\frac{\langle (\partial_x f)^2 - (\partial_y f)^2 \rangle}{\langle (\partial_x f)^2 + (\partial_y f)^2 \rangle + \Delta}$$

$$\gamma_2 = -\frac{\langle \partial_x f \partial_y f \rangle}{\langle (\partial_x f)^2 + (\partial_y f)^2 \rangle + \Delta}$$

$$\Delta = \frac{\beta^2}{2}\langle \vec{\nabla} f \cdot \vec{\nabla}(\nabla^2 f) \rangle$$

(JZ, 2008)

$$\frac{1}{2}\frac{\langle P_{20} - P_{02} \rangle_{en}}{\langle P_{20} + P_{02} - \beta^2 D_4/2 \rangle_{en}} = -\frac{\gamma_1}{1-\kappa} + O(\gamma^3),$$

$$\frac{\langle P_{11} \rangle_{en}}{\langle P_{20} + P_{02} - \beta^2 D_4/2 \rangle_{en}} = -\frac{\gamma_2}{1-\kappa} + O(\gamma^3).$$

$$P_{ij} = \int d^2\vec{k} k_1^i k_2^j \left| \widetilde{f_O}(\vec{k}) \right|^2$$

$$D_n = \int d^2\vec{k} \left| \vec{k} \right|^n \left| \widetilde{f_O}(\vec{k}) \right|^2$$

(JZ, 2011)

$$W_{PSF} = \frac{1}{2\pi\beta^2} \exp\left(-\frac{\left|\vec{\theta}\right|^2}{2\beta^2} \right)$$

The Fourier_Quad Method

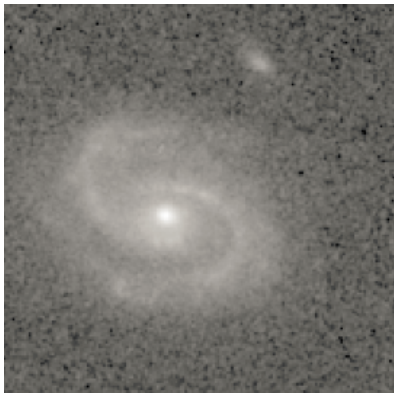

$$\tilde{f}(\vec{k}) = \int d^2\vec{x} e^{i\vec{k}\cdot\vec{x}} f(\vec{x}).$$

From Source Img

From Bkg Img

$$G_1 = -\frac{C}{2}\sum_{j=1}^{N_T}\left[(\vec{k}_j)_x^2 - (\vec{k}_j)_y^2\right] T(\vec{k}_j) M(\vec{k}_j)$$

$$G_2 = -C\sum_{j=1}^{N_T}(\vec{k}_j)_x(\vec{k}_j)_y T(\vec{k}_j) M(\vec{k}_j)$$

$$N = C\sum_{j=1}^{N_T}\left[\left|\vec{k}_j\right|^2 - \frac{\beta^2}{2}\left|\vec{k}_j\right|^4\right] T(\vec{k}_j) M(\vec{k}_j)$$

$$M(\vec{k}) = \left|\tilde{f}^O(\vec{k})\right|^2 + F^O + \left|\tilde{f}^B(\vec{k})\right|^2 + F^B$$

$$F^O = \frac{\sum_{|\vec{k}_j|>k_c}\left|\tilde{f}^O(\vec{k}_j)\right|^2}{\sum_{|\vec{k}_j|>k_c}}, \quad F^B = \frac{\sum_{|\vec{k}_j|>k_c}\left|\tilde{f}^B(\vec{k}_j)\right|^2}{\sum_{|\vec{k}_j|>k_c}}$$

$$\frac{\langle G_1\rangle}{\langle N\rangle} = g_1, \quad \frac{\langle G_2\rangle}{\langle N\rangle} = g_2$$

JZ, Luo, Foucaud, 2015

Test Results

$$g_1^{measured} = (1+m_1)g_1^{input} + c_1$$

$$g_2^{measured} = (1+m_2)g_2^{input} + c_2$$

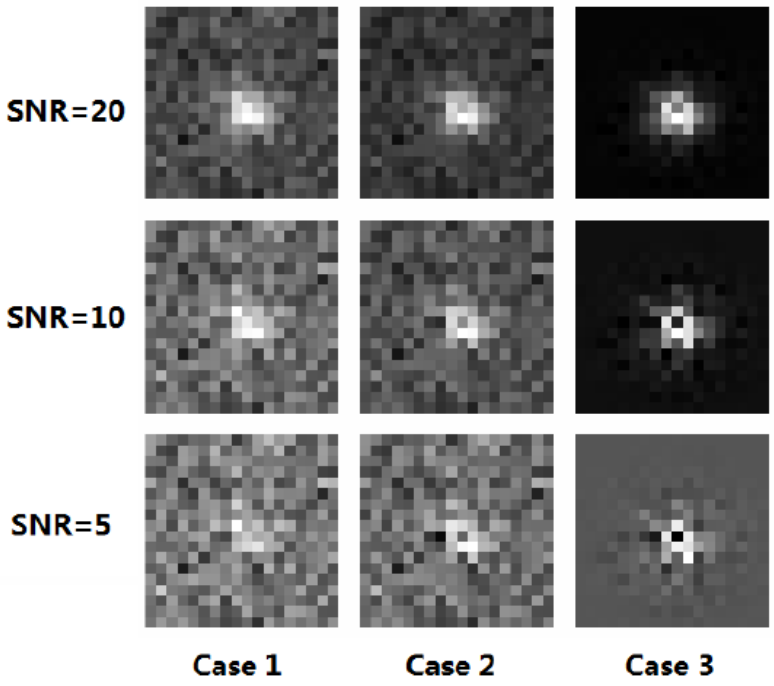

	Case 1	Case 2	Case 3
SNR= 20	$m_1(10^{-3}) : -0.2 \pm 0.2$	-0.2 ± 0.1	-0.08 ± 0.05
	$c_1(10^{-5}) : -1.0 \pm 0.7$	-0.6 ± 0.4	0.0 ± 0.2
SNR= 10	-0.6 ± 0.6	-0.4 ± 0.4	-0.1 ± 0.1
	-2.6 ± 2.1	-1.6 ± 1.2	0.0 ± 0.4
SNR= 5	-2.2 ± 2.3	-1.1 ± 1.2	0.0 ± 0.2
	-7.9 ± 7.9	-4.6 ± 4.1	0.1 ± 0.8
SNR= 20	$m_2(10^{-3}) : -0.2 \pm 0.2$	-0.3 ± 0.1	-0.3 ± 0.05
	$c_2(10^{-5}) : 1.4 \pm 0.7$	1.1 ± 0.4	0.3 ± 0.2
SNR= 10	-0.3 ± 0.6	-0.4 ± 0.4	-0.4 ± 0.1
	3.7 ± 2.1	2.6 ± 1.2	0.6 ± 0.4
SNR= 5	-0.7 ± 2.3	-0.9 ± 1.2	-0.6 ± 0.2
	10.6 ± 7.9	6.6 ± 4.1	1.2 ± 0.8

JZ et al., 2015

Team	Class	Weighting scheme	Calibration philosophy	Limitations	$N_{\rm branch}$	Rank	Exact PSF?	New software	Time per galaxy
Amalgam@IAP	Maximum likelihood	Inverse variance	Ellipticity penalty	None	16	2	Yes	Some	0.1–1 s
BAMPenn	Bayesian Fourier	Implicit	$p(\varepsilon)$ from deep data	Variable shear	2	-	Yes	Yes	< 1 s
EPFL_glfit	Maximum likelihood	Constant + rejection	None	None	8	6	Yes	Yes	1–3 s
CEA-EPFL	Maximum likelihood	Various	None	None	20	3	Yes	Yes	1–3 s
CEA_denoise	Moments	Constant	None	None	8	-	Yes	No	0.03 s
CMU experimenters	Stacking	Constant	External simulations	Variable shear	2	N/A	Yes	Some	0.03 s
COCS (IM3SHAPE)	Maximum likelihood	Constant	External simulations	None	12	N/A	Yes	Yes	1 s
E-HOLICS	Moments	Constant + rejection	External simulations	None	12	8	Yes	No	1–3 s
EPFL_HNN	Neural network	Constant	None	None	7	-	Yes	Yes	2-3 s
EPFL_KSB	Moments	Inverse variance	None	None	4	-	Yes	No	0.001-0.002 s
EPFL_MLP / EPFL_MLP_FIT	Neural network	Constant	None	None	5	-	Yes	Yes	2-3 s
FDNT	Fourier moments	Inverse variance	External simulations	None	12	N/A	Yes	Some	~ 1 s
Fourier_Quad	Fourier moments	Various	None	None	6	5	Yes	No	0.001-0.002 s
HSC/LSST-HSM	Moments	Inverse variance	External simulations	None	4	N/A	Yes	Some	0.05 s
MBI	Bayesian hierarchical	Implicit	Inferred $p(\varepsilon)$	Variable shear, PSF	4	9	No	Some	10 s
MaltaOx (LENSFIT)	Partially Bayesian	Inverse variance	Self-calibration	None	3	7	Yes	Some	0.05 s
MegaLUT	Supervised ML	Constant + rejection	External simulations	None	16	4	Yes	Some	0.02 s
MetaCalibration	Moments + self-calibration	Inverse variance	Self-calibration	Variable shear	1	N/A	Yes	Yes	0.3 s
Wentao_Luo	Moments	Inverse variance	None	None	4	-	Yes	Yes	1-2 s
ess	Bayesian model-fitting	Implicit	$p(\varepsilon)$ from deep data	Variable shear	2	-	No	Yes	1 s
sFIT	Maximum likelihood	Inverse variance	External simulations (iterative)	None	20	1	Yes	Yes	0.8 s

Mandelbaum et al. (2015)

Regarding the way of doing shear statistics

$$\epsilon_1,\ \epsilon_2,\ w$$

Conventional Form:

$$g_1 = \frac{\sum_i \epsilon_1(i) w(i)}{\sum_i w(i)}$$

$$\langle g_1(\vec{x}) g_1(\vec{x}+\vec{r})\rangle = \left.\frac{\sum_{ij} \epsilon_1(i)\epsilon_1(j) w(i) w(j)}{\sum_{ij} w(i) w(j)}\right|_{\vec{x}_j - \vec{x}_i = \vec{r}}$$

$$G_1,\ G_2,\ N$$

New Form:

$$g_1 = \frac{\sum_i G_1(i)}{\sum_i N(i)}$$

$$\langle g_1(\vec{x}) g_1(\vec{x}+\vec{r})\rangle = \left.\frac{\sum_{ij} G_1(i) G_1(j)}{\sum_{ij} N(i) N(j)}\right|_{\vec{x}_j - \vec{x}_i = \vec{r}}$$

Regarding the way of doing shear statistics

Order One $\epsilon_1,\ \epsilon_2$ w **Nonnegative**

Conventional Form:

$$g_1 = \frac{\sum_i \epsilon_1(i) w(i)}{\sum_i w(i)}$$

$$\langle g_1(\vec{x}) g_1(\vec{x}+\vec{r})\rangle = \left.\frac{\sum_{ij} \epsilon_1(i)\epsilon_1(j) w(i) w(j)}{\sum_{ij} w(i) w(j)}\right|_{\vec{x}_j - \vec{x}_i = \vec{r}}$$

$G_1,\ G_2,\ N$ **~ 0± for faint sources**

New Form:

$$g_1 = \frac{\sum_i G_1(i)}{\sum_i N(i)}$$

$$\langle g_1(\vec{x}) g_1(\vec{x}+\vec{r})\rangle = \left.\frac{\sum_{ij} G_1(i) G_1(j)}{\sum_{ij} N(i) N(j)}\right|_{\vec{x}_j - \vec{x}_i = \vec{r}}$$

Approaching the C-R Bound in Shear Statistics

With PDF Symmetrization: $G_i - \hat{g}_i N$

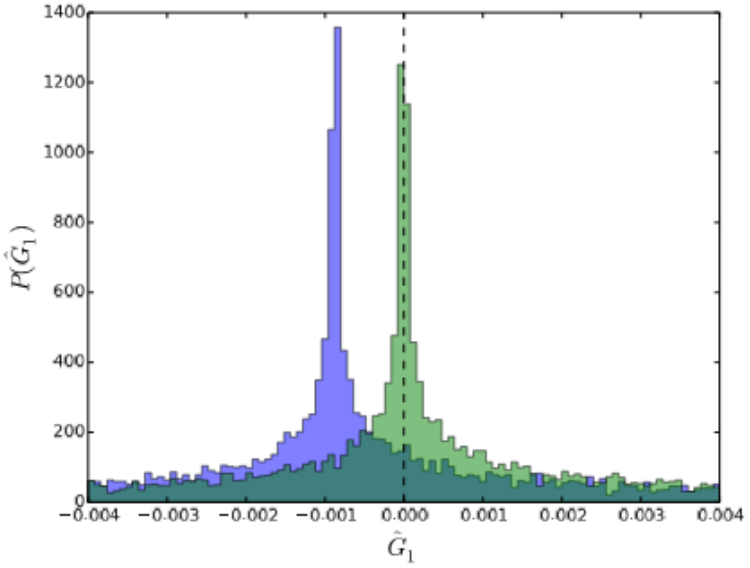

Method	$g_1(-0.018)$	$g_2(0.011)$
Direct Averaging	−0.017(2)	0.011(2)
PDF-SYM (2 bins)	−0.01798(3)	0.01100(2)
PDF-SYM (4 bins)	−0.01799(2)	0.01102(2)
PDF-SYM (8 bins)	−0.01800(2)	0.01101(2)

JZ, Zhang, Luo, 2017, ApJ, 834, 8

APPROACHING THE CRAMER-RAO BOUND IN WEAK LENSING WITH PDF SYMMETRIZATION

C-R BOUND

$$0 = \frac{d}{d\hat{g}} \sum_i \ln P(x_i - \hat{g})$$

$$\sigma_{\hat{g}}^{-2} = -\sum_i \frac{\partial^2 \ln P(x_i - \hat{g})}{\partial \hat{g}^2}$$

Examples

$$P_1(x) = \frac{1}{\sqrt{2\pi}} \exp\left(-\frac{x^2}{2}\right)$$

$$P_2(x) = \frac{2}{\pi}(1+x^2)^{-2}$$

$$P_3(x) = \frac{|x|^{-2/3}}{3\sqrt{2\pi}} \exp\left(-\frac{|x|^{2/3}}{2}\right)$$

$$N_T\sigma_1^2(\mathrm{Ave}) = 1, \quad N_T\sigma_1^2(\mathrm{CR}) = 1,$$
$$N_T\sigma_2^2(\mathrm{Ave}) = 1, \quad N_T\sigma_2^2(\mathrm{CR}) = 0.5,$$
$$N_T\sigma_3^2(\mathrm{Ave}) = 15, \quad N_T\sigma_3^2(\mathrm{CR}) \to 0.$$

The results of signal recovery (input value is 0.01) for 10^7 data points of three types of PDF's

Results:	Averaging	PDF-SYM (2 bins)	PDF-SYM (8 bins)	PDF-SYM (16 bins)	PDF-SYM (32 bins)
P_1	0.0102(3)	0.0104(4)	0.0101(3)	0.0100(4)	0.0102(3)
P_2	0.0099(3)	0.0101(2)	0.0101(2)	0.0100(2)	0.0101(2)
P_3	0.011(1)	0.0099999998(2)	0.0099999998(1)	0.0099999998(1)	0.0099999999(2)

$N_T\sigma^2$:	Averaging	PDF-SYM (2 bins)	PDF-SYM (8 bins)	PDF-SYM (16 bins)	PDF-SYM (32 bins)
P_1	1.0	1.6	1.1	1.2	0.96
P_2	0.99	0.61	0.52	0.50	0.57
P_3	15	5×10^{-13}	2×10^{-13}	2×10^{-13}	3×10^{-13}

JZ, Zhang, Luo, 2017, ApJ, 834, 8

APPROACHING THE CRAMER-RAO BOUND IN WEAK LENSING WITH PDF SYMMETRIZATION

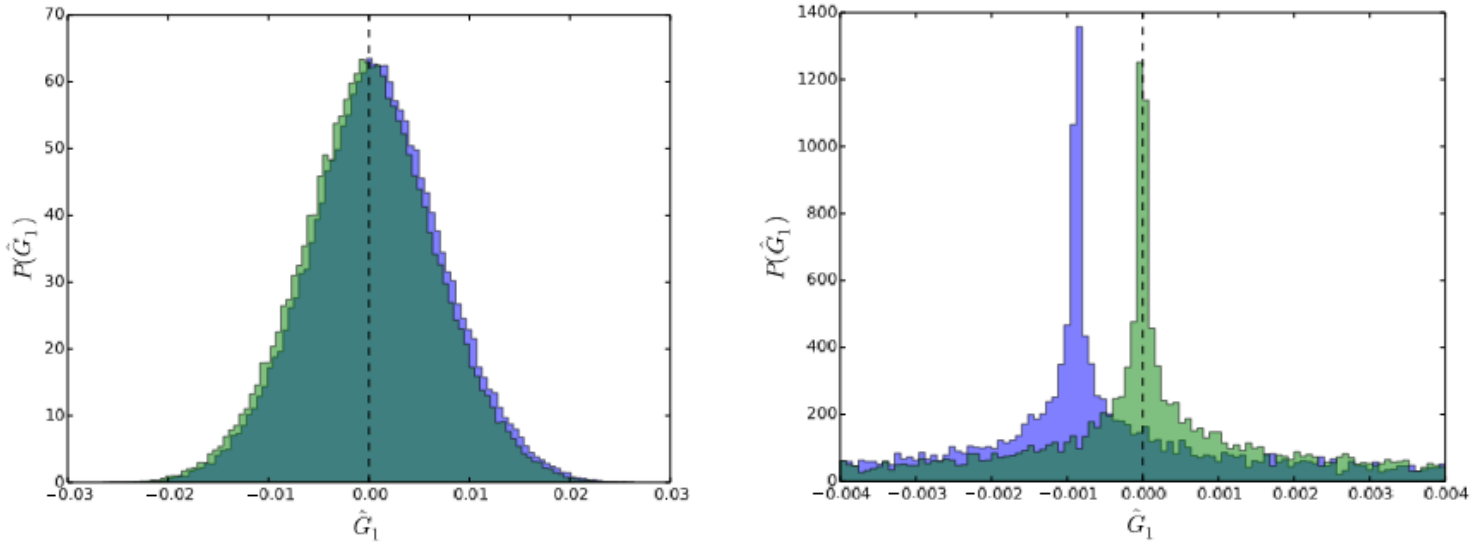

$g_1 = 0.02277,\ g_2 = -0.01386$

Results of $[g_1, g_2]$:	10^5 RW Galaxies	9×10^4 RW+10^4 Ring
Averaging	$[0.0226(6), -0.0130(6)]$	$[0.0231(6), -0.0132(6)]$
PDF-SYM (8 bins)	$[0.0225(7), -0.0129(6)]$	$[0.02278(8), -0.01392(7)]$

JZ, Zhang, Luo, 2017, ApJ, 834, 8

APPROACHING THE CRAMER-RAO BOUND IN WEAK LENSING WITH PDF SYMMETRIZATION

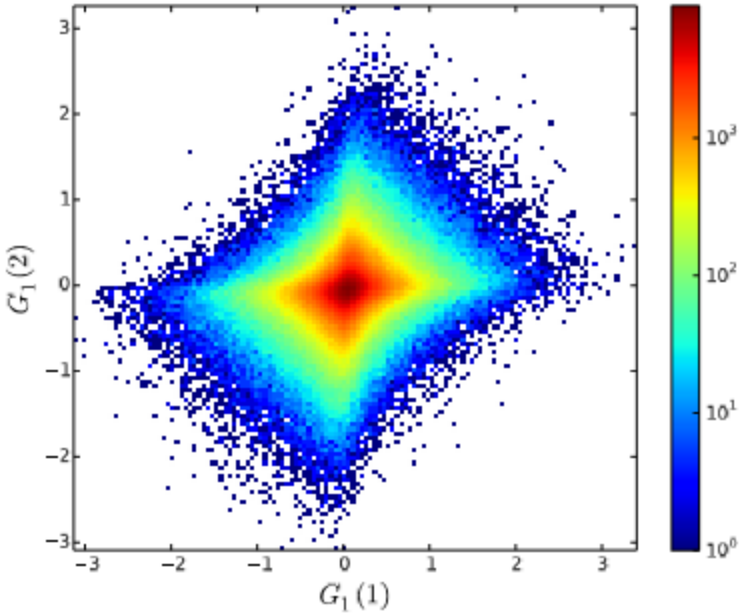

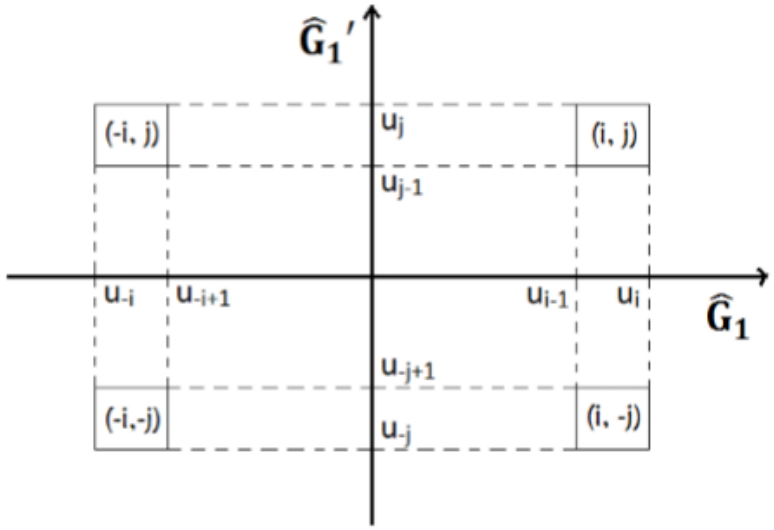

The recovered shear-shear correlations. The inputs are $\langle g_t^{(1)} g_t^{(2)} \rangle = 10^{-4}$ and $\langle g_\times^{(1)} g_\times^{(2)} \rangle = -10^{-4}$.

Results of $[\langle g_t^{(1)} g_t^{(2)} \rangle, \langle g_\times^{(1)} g_\times^{(2)} \rangle](10^{-4})$:	Averaging	PDF-SYM (8×8 bins)
4×10^7 RW Gal. Pairs	$[1.09(8), -1.00(8)]$	$[1.09(8), -1.01(9)]$
4×10^7 Ring Gal. Pairs	$[1.05(7), -1.08(7)]$	$[1.002(5), -1.002(5)]$
4×10^7 Gal. Pairs with 90% RW and 10% Ring	$[1.09(8), -1.02(8)]$	$[0.99(3), -1.00(3)]$
1.6×10^8 Ring Gal. Pairs with noise and 10% stars	$[0.97(4), -1.05(4)]$	$[1.000(3), -1.001(3)]$

JZ, Zhang, Luo, 2017, ApJ, 834, 8

History of Fourier_Quad

1. JZ, MNRAS, 383, 113 (2008) Correct for the PSF effect model-independently;
2. JZ, MNRAS, 403, 673 (2010) Remove the background noise contamination;
3. JZ, JCAP, 11, 041 (2011) Clarify the impact of pixel size and high order terms;
4. JZ, Komatsu, MNRAS, 414, 1047 (2011) The correct form of shear estimator;
5. JZ, Luo, Foucaud, JCAP, 01, 024 (2015) Correct for the Poisson noise;
6. JZ, Zhang, Luo, ApJ, 834, 8 (2017) A novel way of doing shear statistics to approach the Cramer-Rao bound.

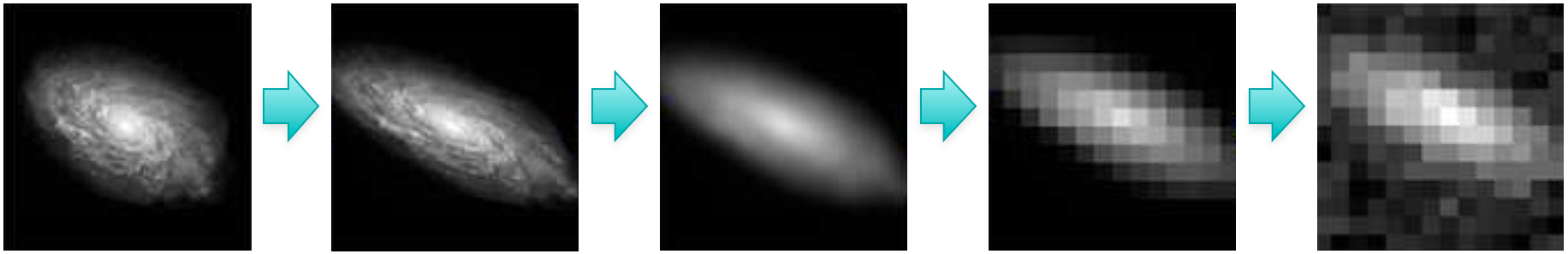

Lensing PSF Pixelation Noise

√ √ √

Application on the CFHTLenS data

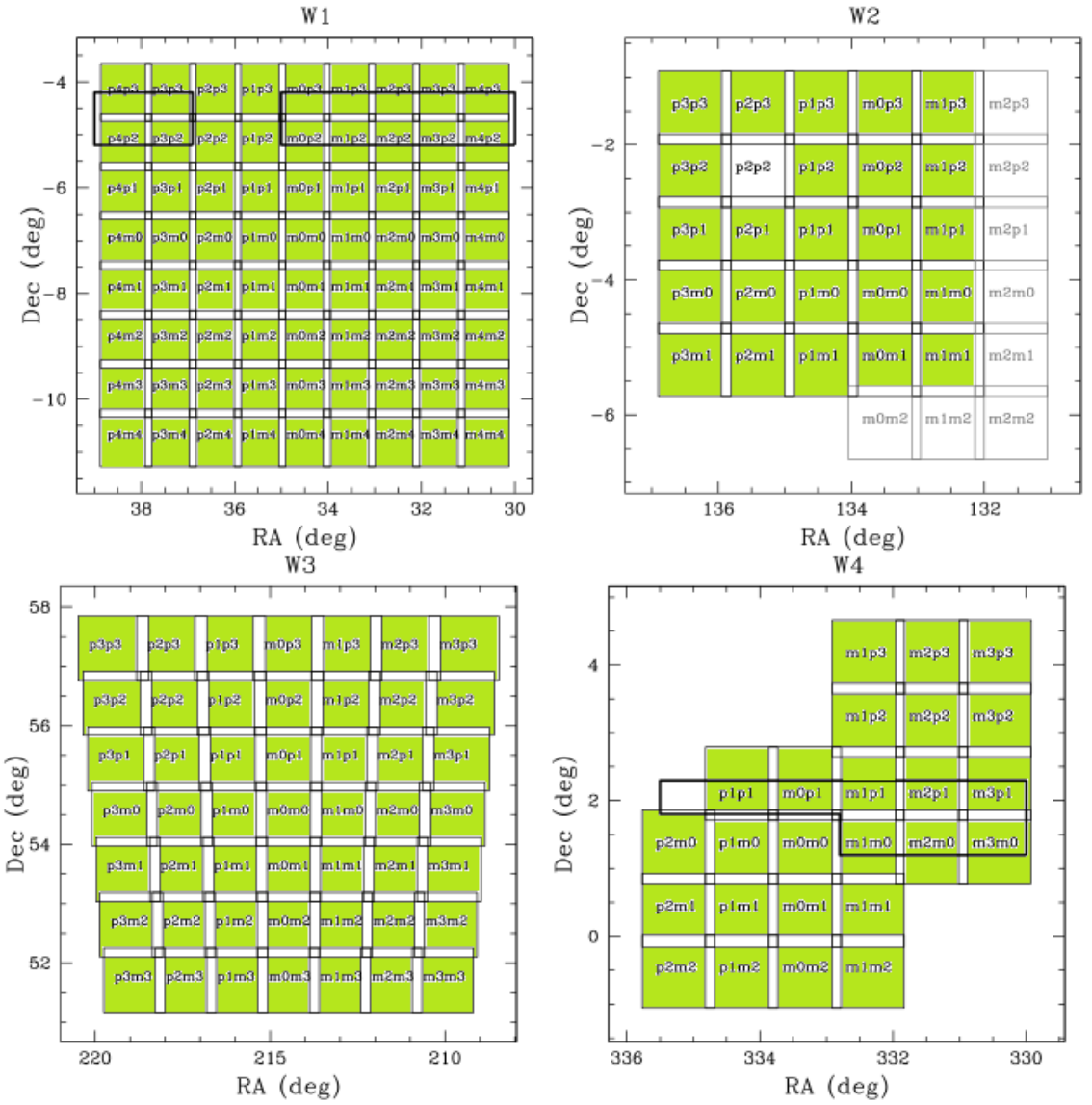

- CFHTLenS

Table 1. Characteristics of the final CFHTLenS co-added science data (see the text for an explanation of the columns).

Filter	expos. time [s]	$m_{\rm lim}$ [AB mag] 5-σ lim. mag. in a 2″.0 aperture	seeing [″]
$u^*(u.MP9301)$	5×600 (3000)	25.24 ± 0.17	0.88 ± 0.11
$g'(g.MP9401)$	5×500 (2500)	25.58 ± 0.15	0.82 ± 0.10
$r'(r.MP9601)$	4×500 (2000)	24.88 ± 0.16	0.72 ± 0.09
$i'(i.MP9701)$	7×615 (4305)	24.54 ± 0.19	0.68 ± 0.11
$y'(i.MP9702)$	7×615 (4305)	24.71 ± 0.13	0.62 ± 0.09
$z'(z.MP9801)$	6×600 (3600)	23.46 ± 0.20	0.70 ± 0.12

- http://www.cfhtlens.org
- Erben et al (2012)
- Heymans et al (2012)
- Miller et al (2012)

Shear Measurement Pipeline Construction

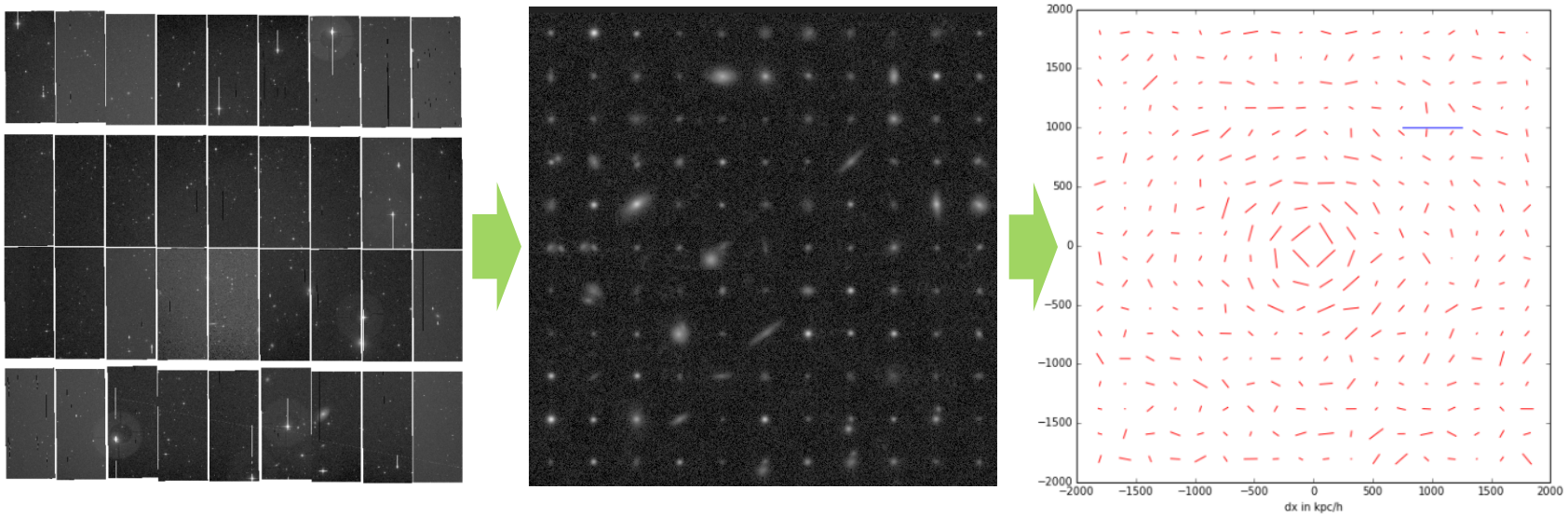

Single Exposure **Source catalog** **Shear Catalog**

We have developed an accurate shear measurement pipeline. Starting with almost raw CCD images (after flat-fielding correction), our code does background removal, masking, astrometric calibration, cosmic ray identification, source selection, PSF reconstruction, shear measurement, etc.. The overall speed is around 0.02 CPU•sec/galaxy, which is about 100 times faster than typical model-fitting methods.

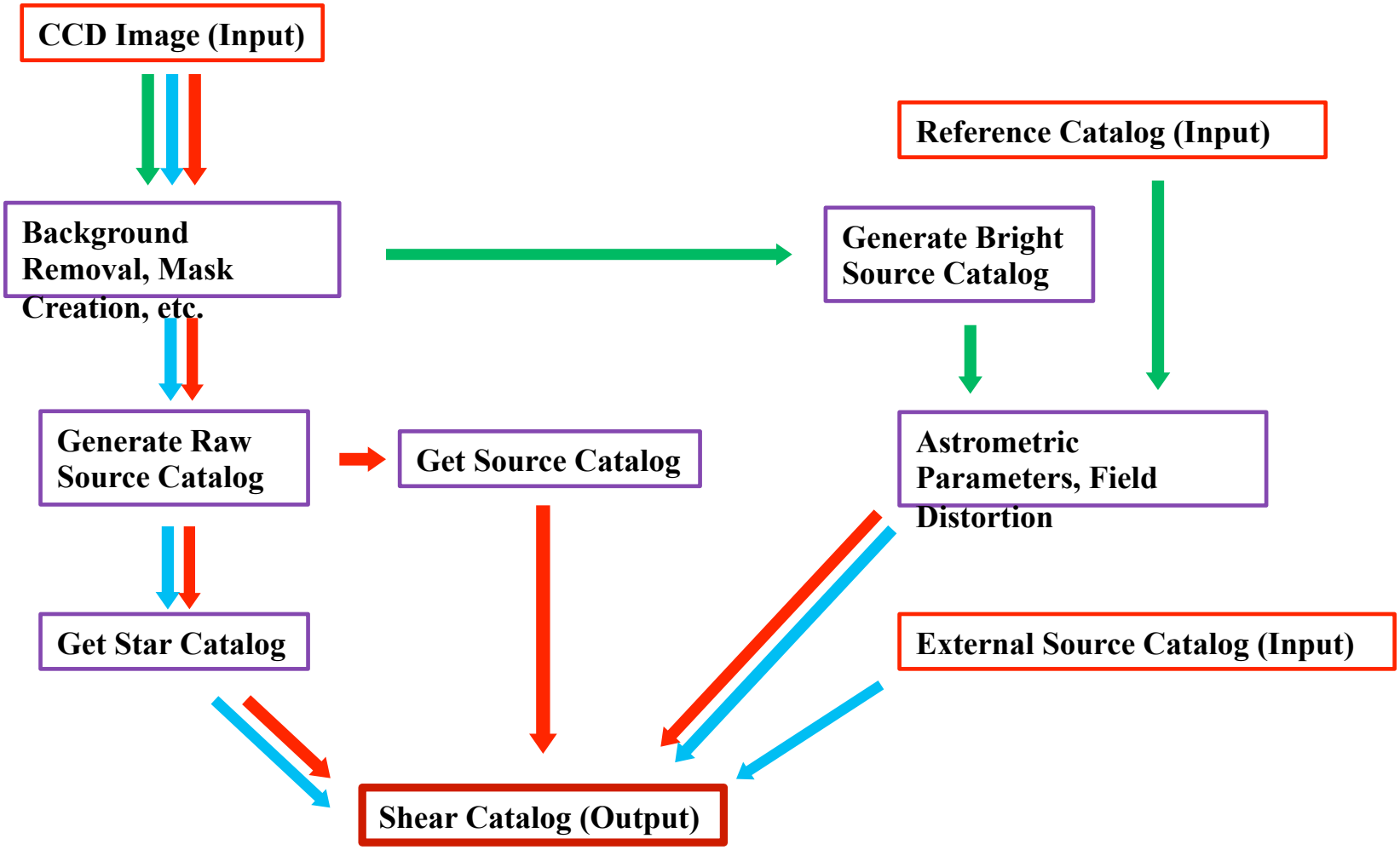

*1. route green: generate astrometric parameters;
*2. route red: generate shear catalog using internal source catalog;
*3. route blue: generate shear catalog using external source catalog.

Problems in Background Removal

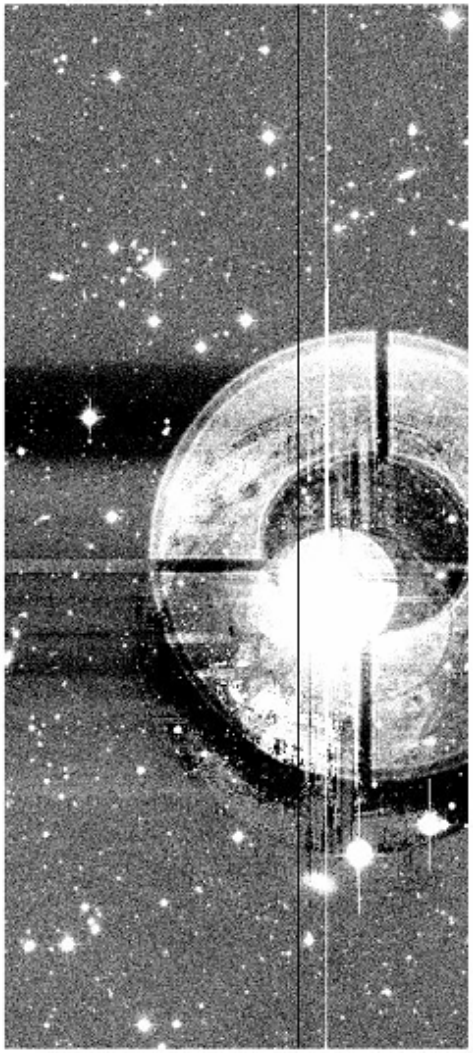

THELI Processed

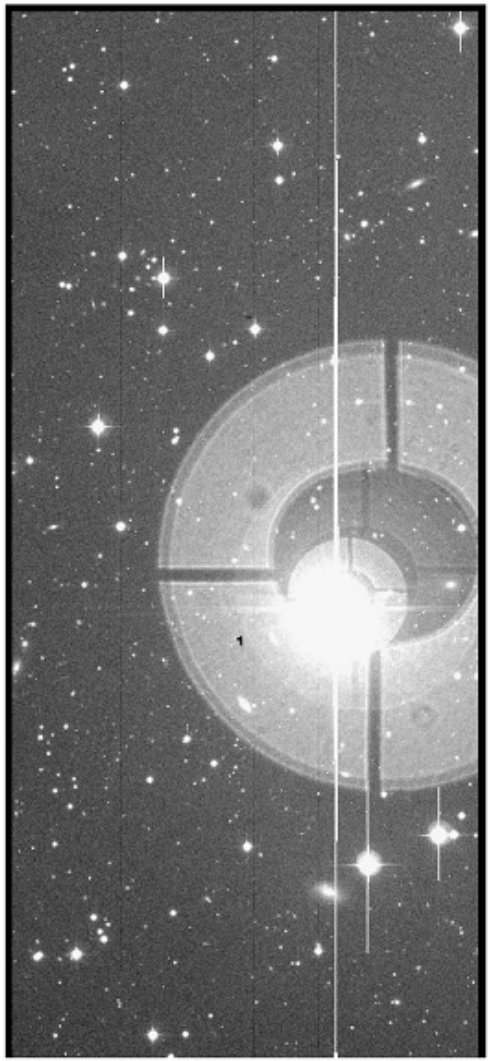

Original Image

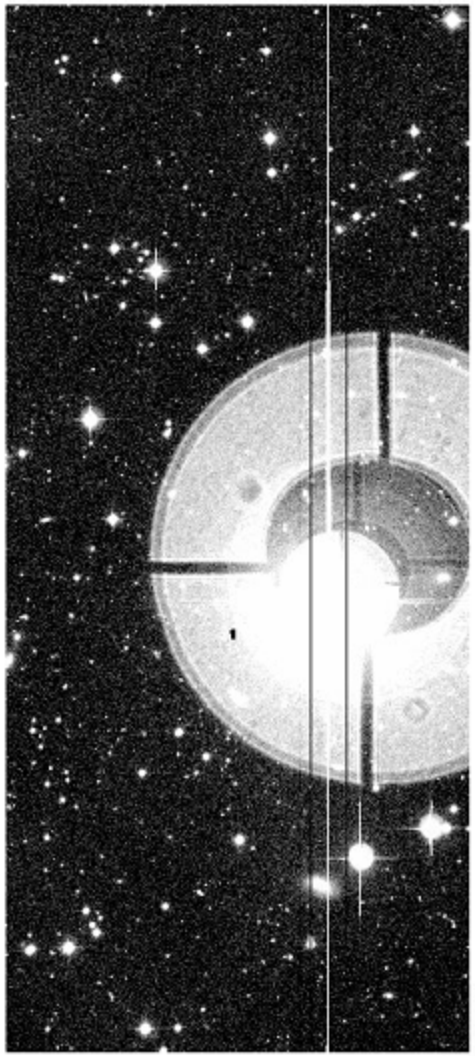

We Processed

Accuracy of Astrometry

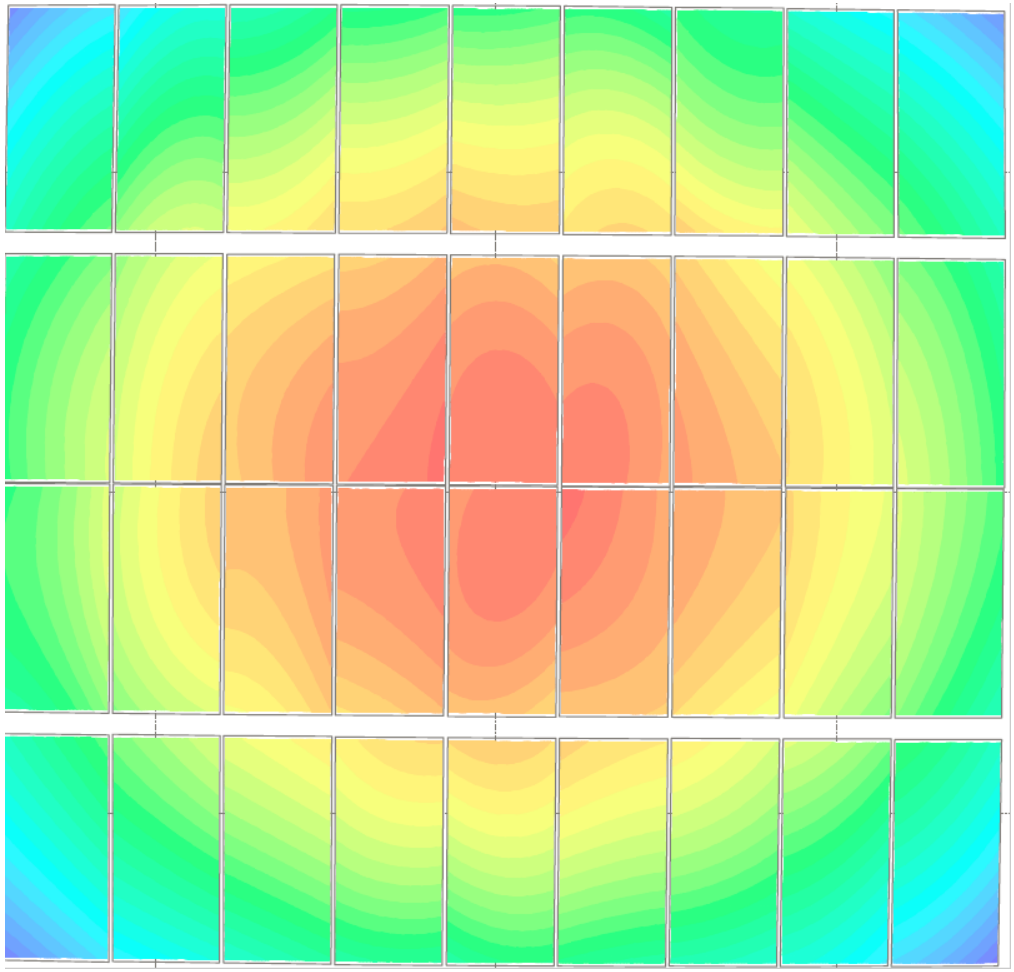

Accuracy of Astrometry (with our code)

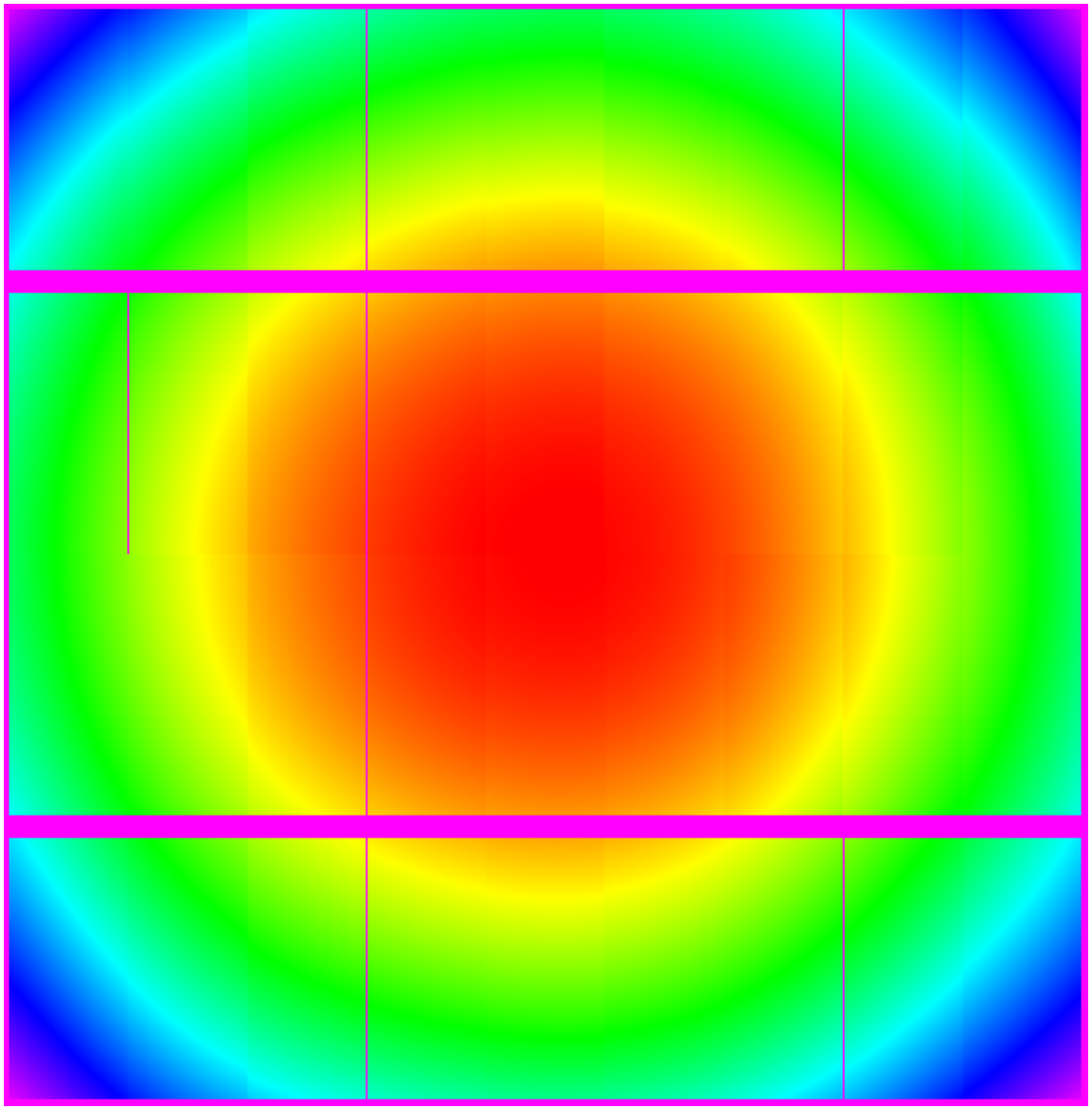

PSF Reconstruction (Find Bright Stars , Build PSF)

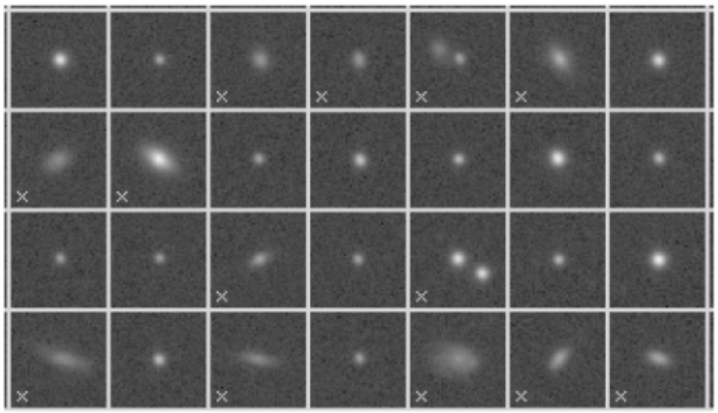

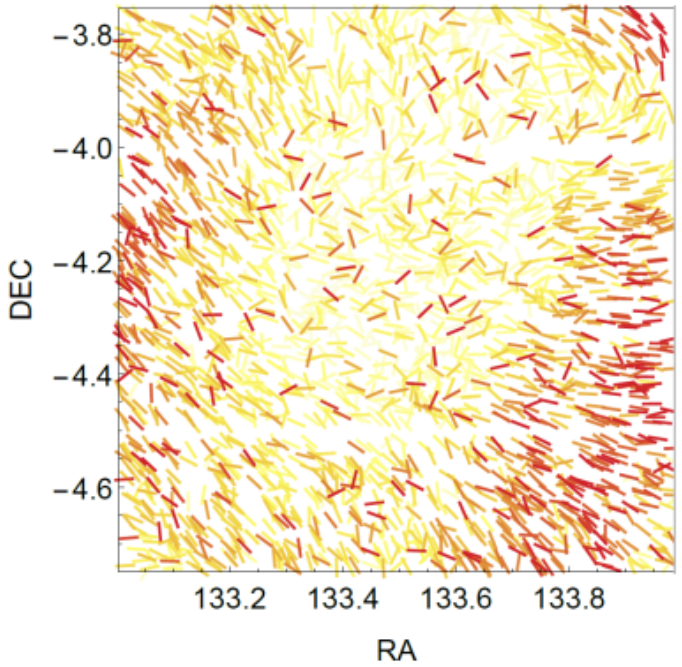

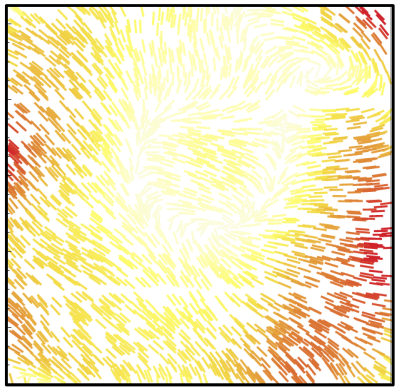

Global Polynomial n = 10

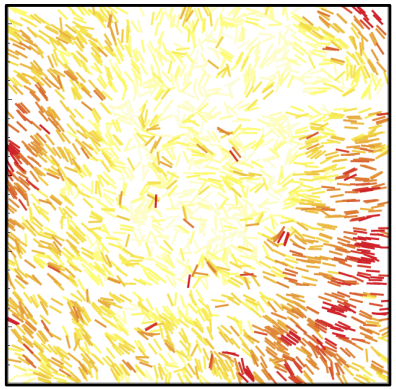

Kriging

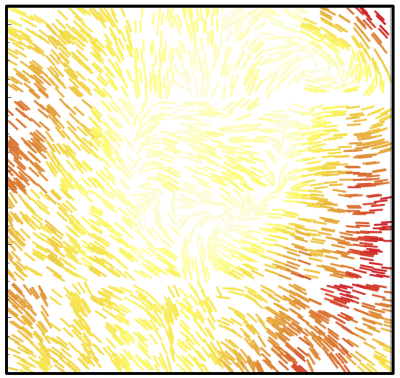

Chipwise Polynomial n = 1

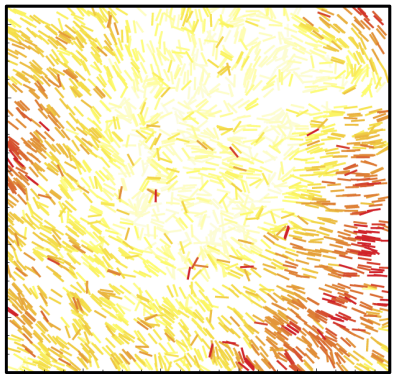

Shepard

Lu, et al. , 2017, AJ, 153, 197

Test Shear Recovery with Field Distortion

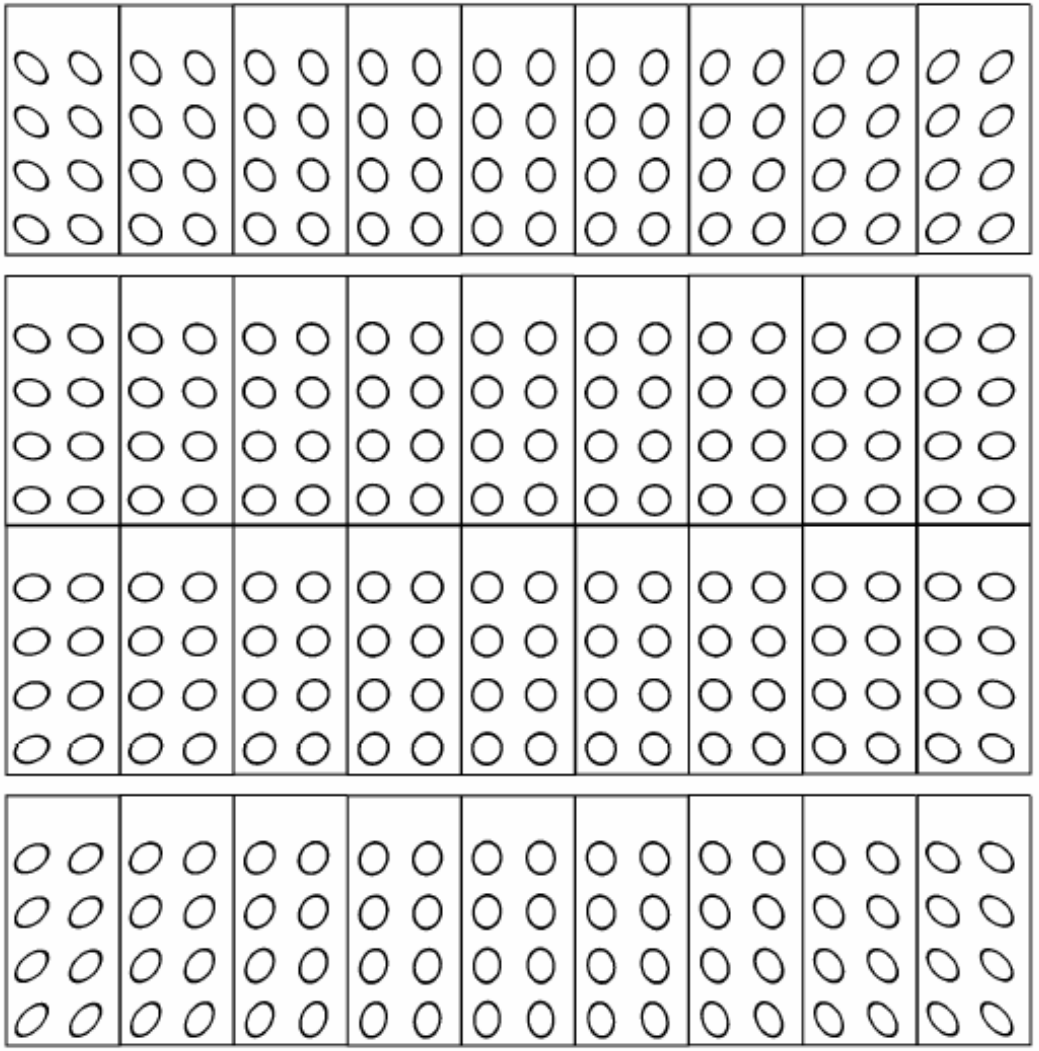

JZ et al., 2019

FD distribution on MegaCam, enlarged by 30 times.

Test Shear Recovery with Field Distortion

With our own source catalog

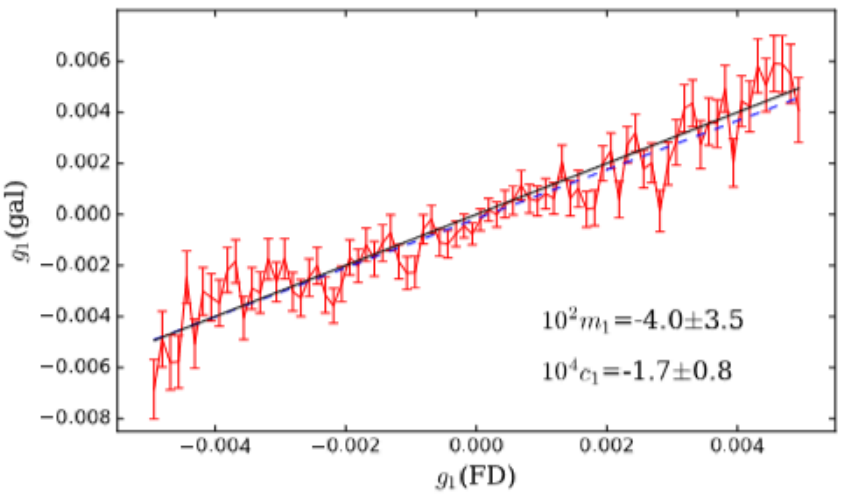

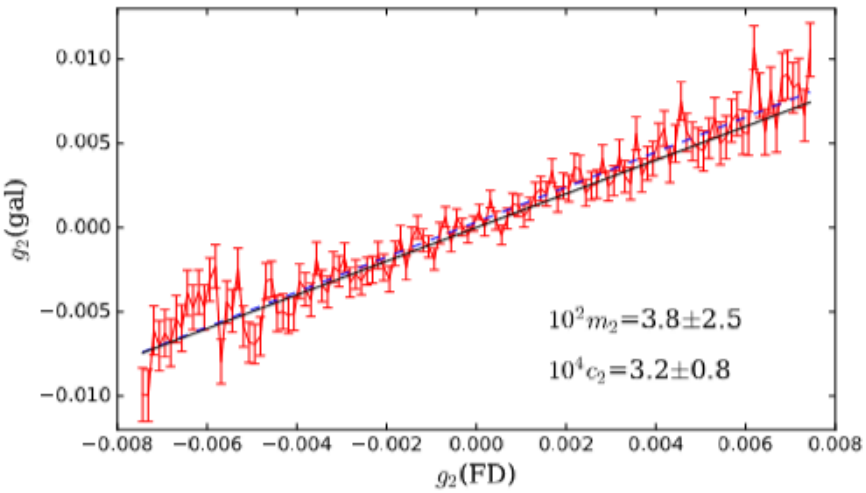

With CFHTLenS source catalog

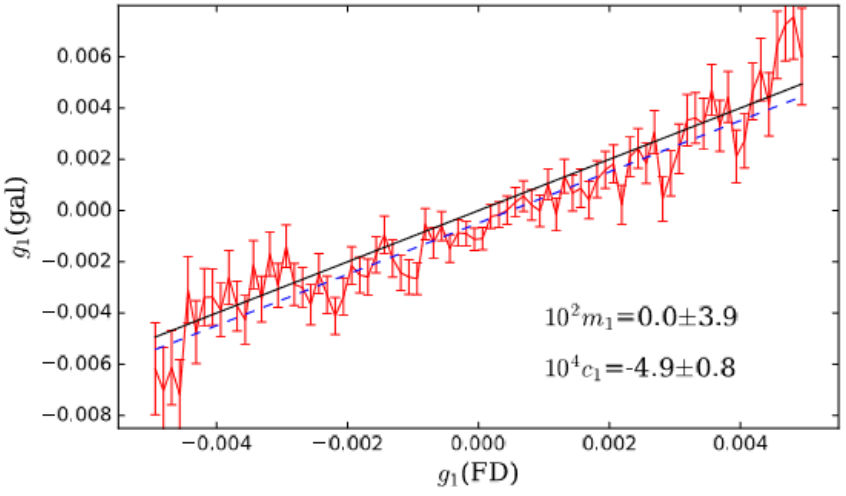

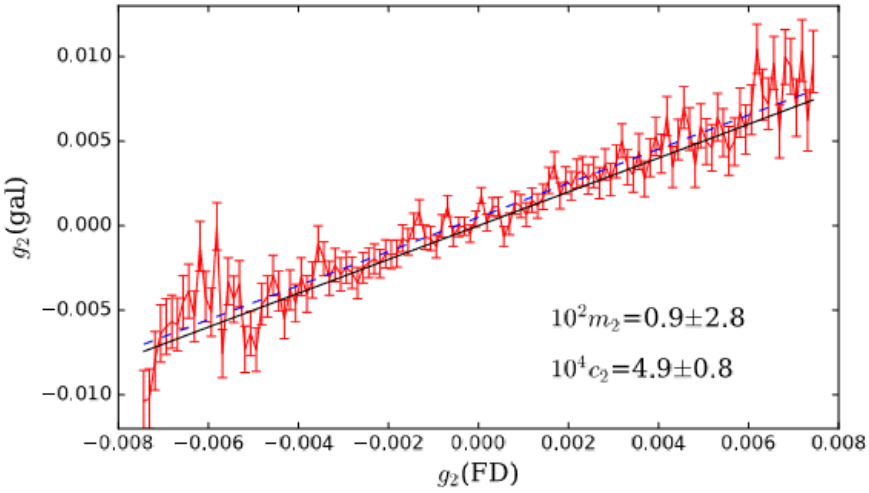

JZ et al., 2019, ApJ, 875, 48

Comparison with Lensfit

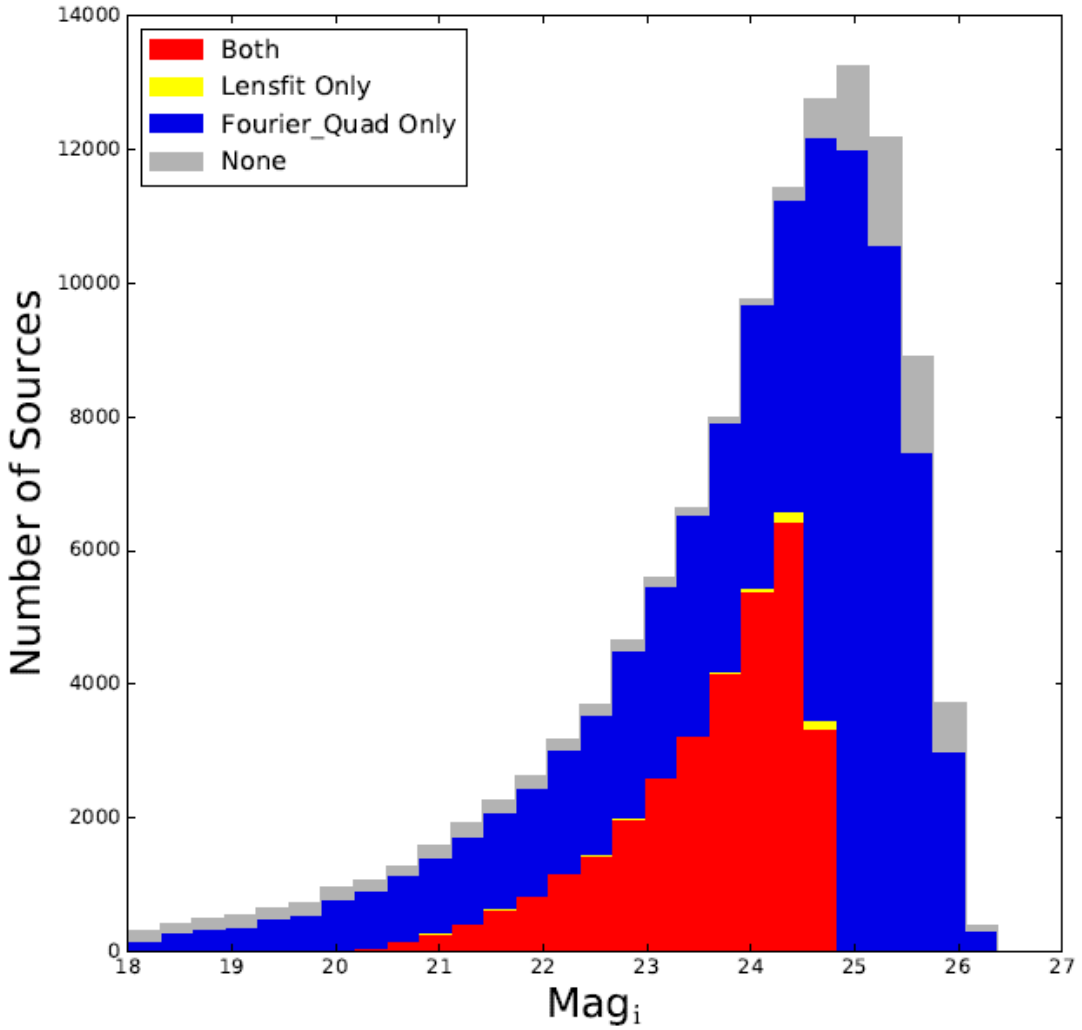

Shear-Shear Tomography

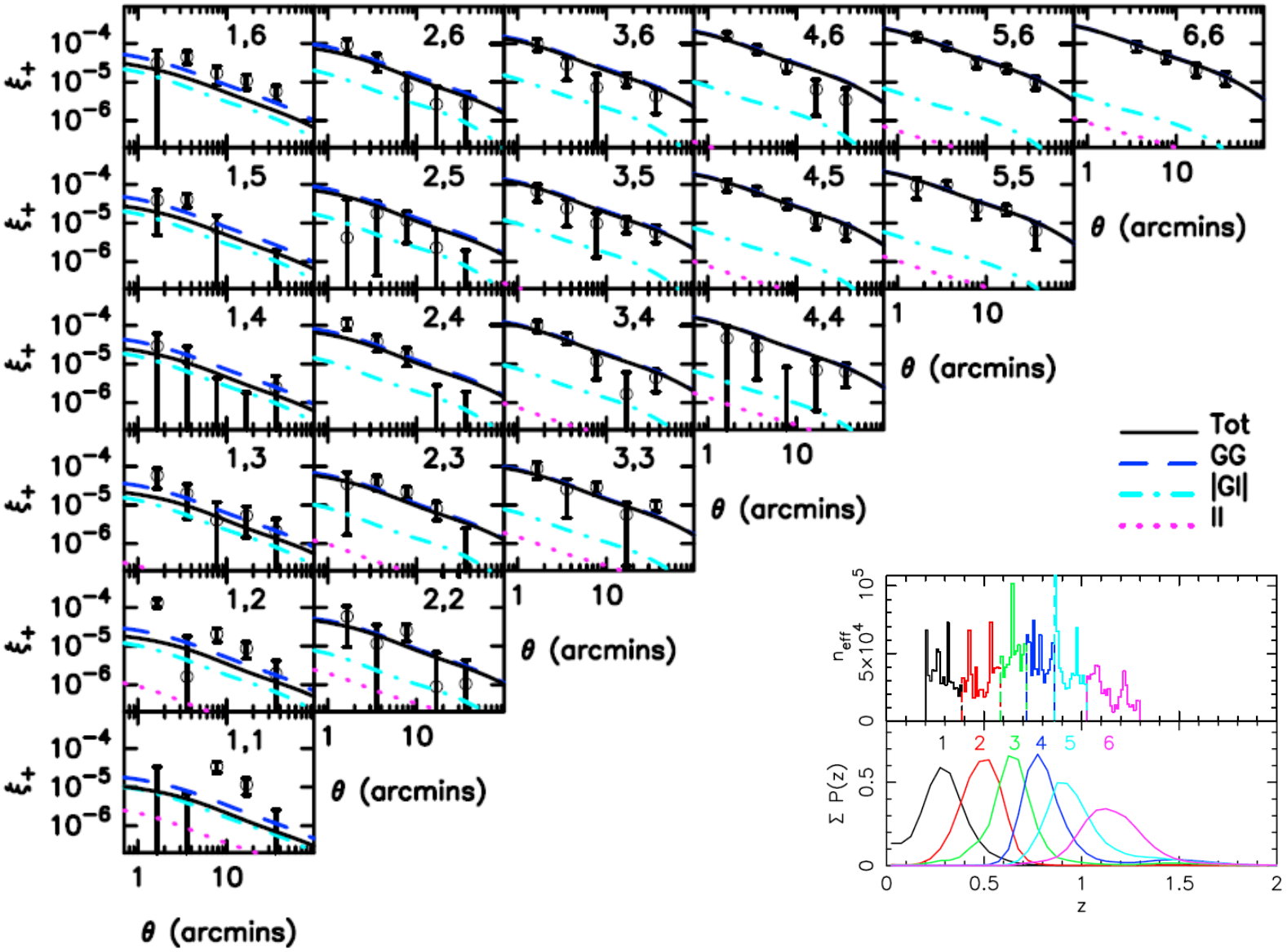

Heymans et al, MNRAS, 432, 2433 (2013)

Shear-Shear Tomography (preliminary)

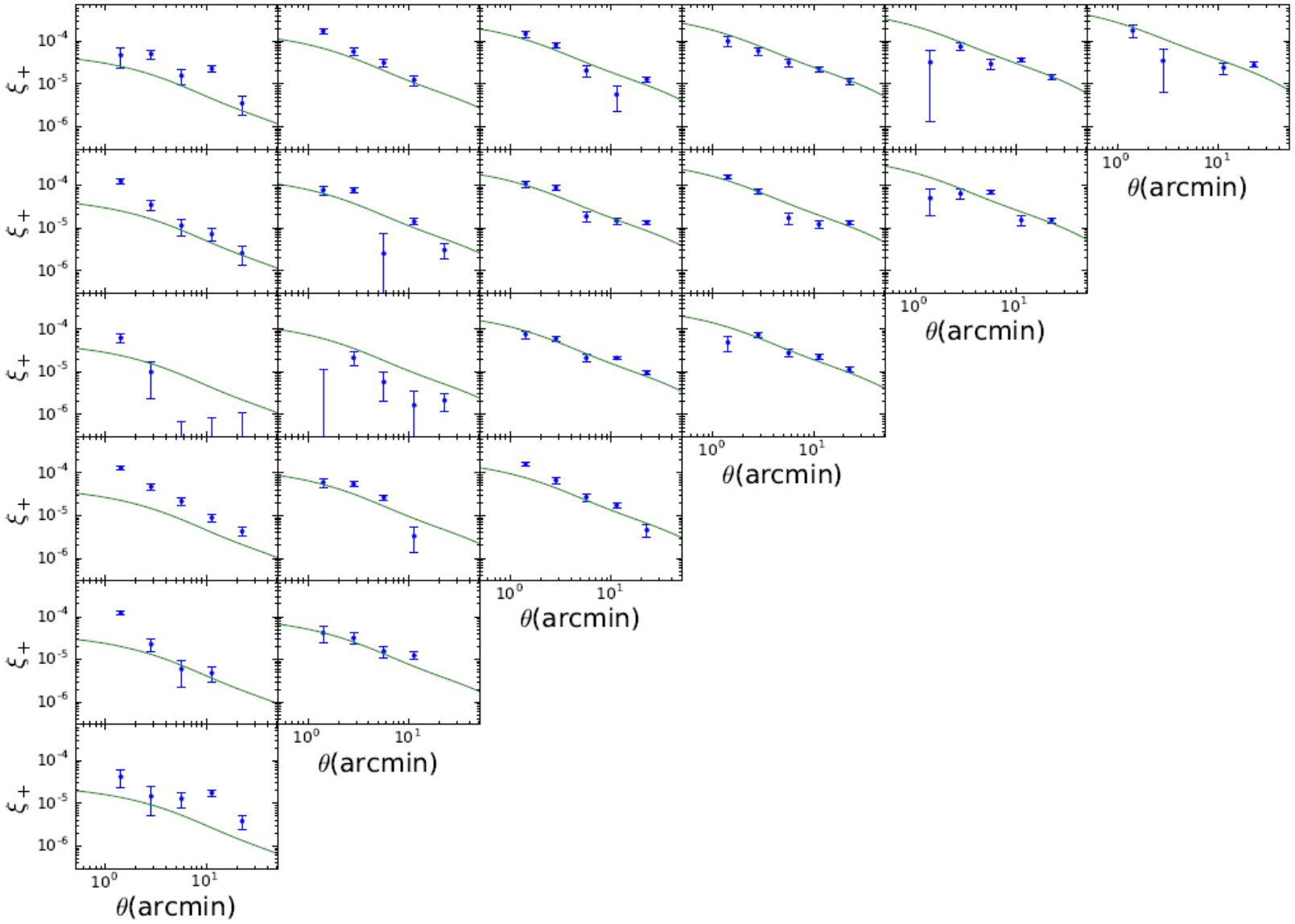

Using BASS data to measure cosmic shear

Regarding Image Quality

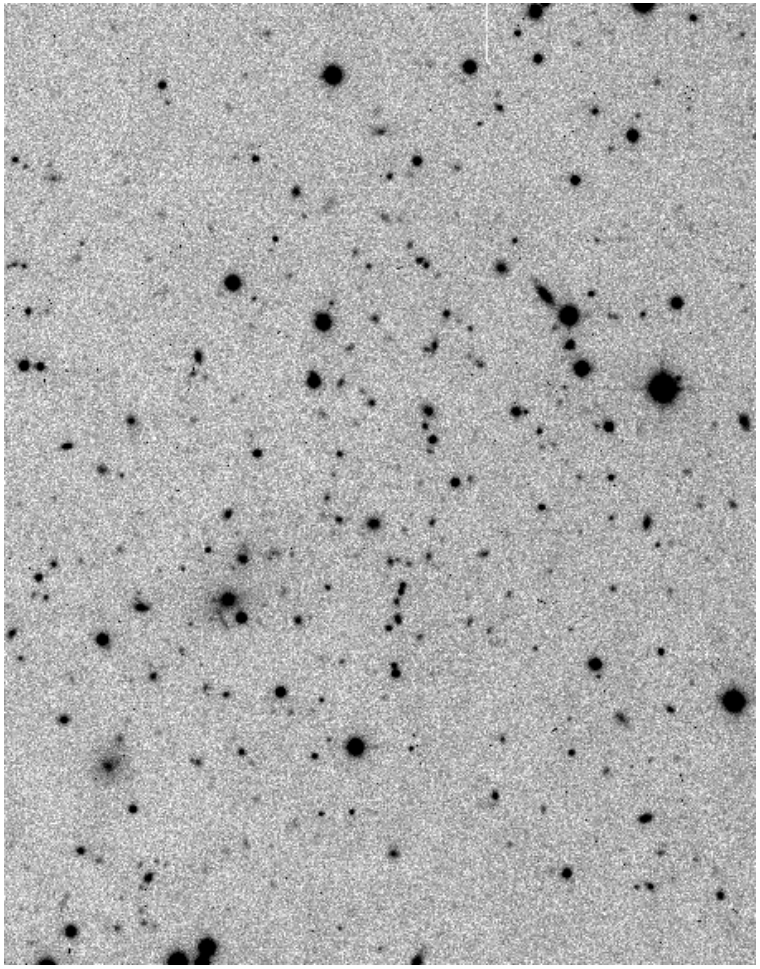

CFHTLenS Exposure

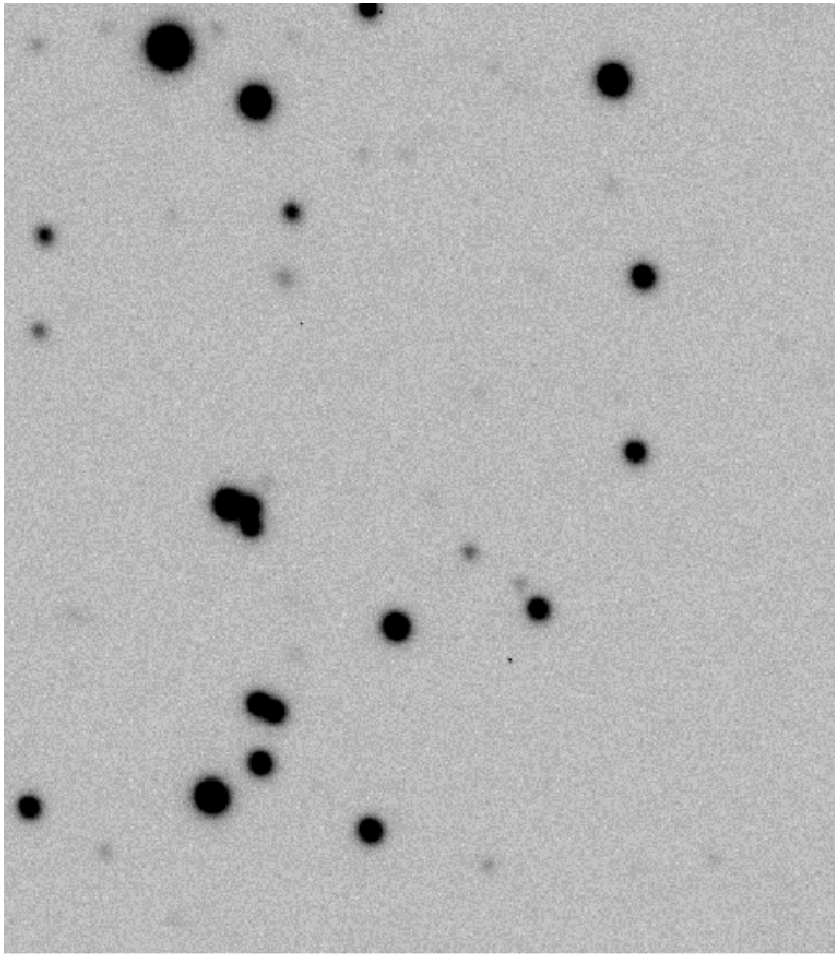

BASS Exposure

Field Distortion Test with BASS Data

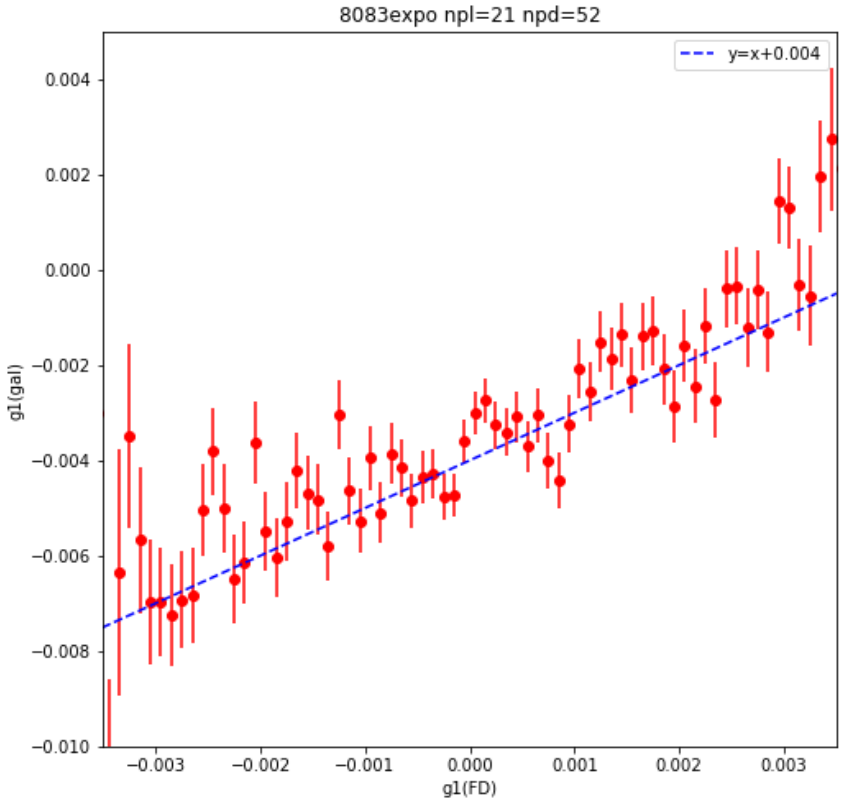

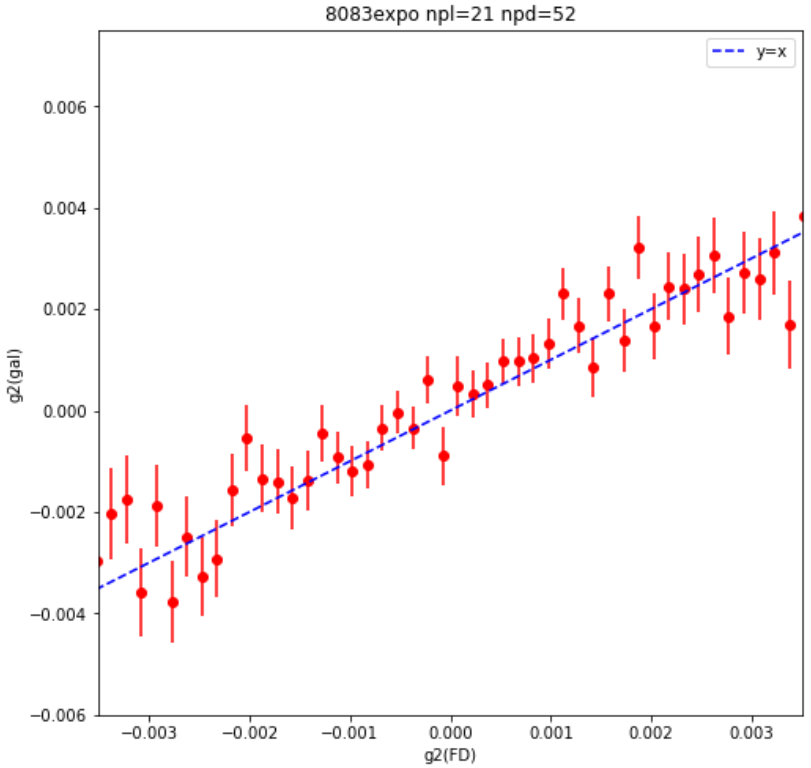

credit：Chunxiang Wang (NAOC)

Outline:

- Progresses
- Concerns

Outline:

- Progresses
- Concerns
  1. Pixelisation Effect;
  2. PSF Reconstruction;
  3. Deblending, Selection Bias;
  4. CCD Effect (CTI, Brighter Fatter, Small Scale Flat-Field Correction)
  5. Astrometric Calibration
  6. Survey Strategy (Stellar density, Targets of interests, Synergy between CSST and Euclid)
  7. ... ...

Pixelisation Effect

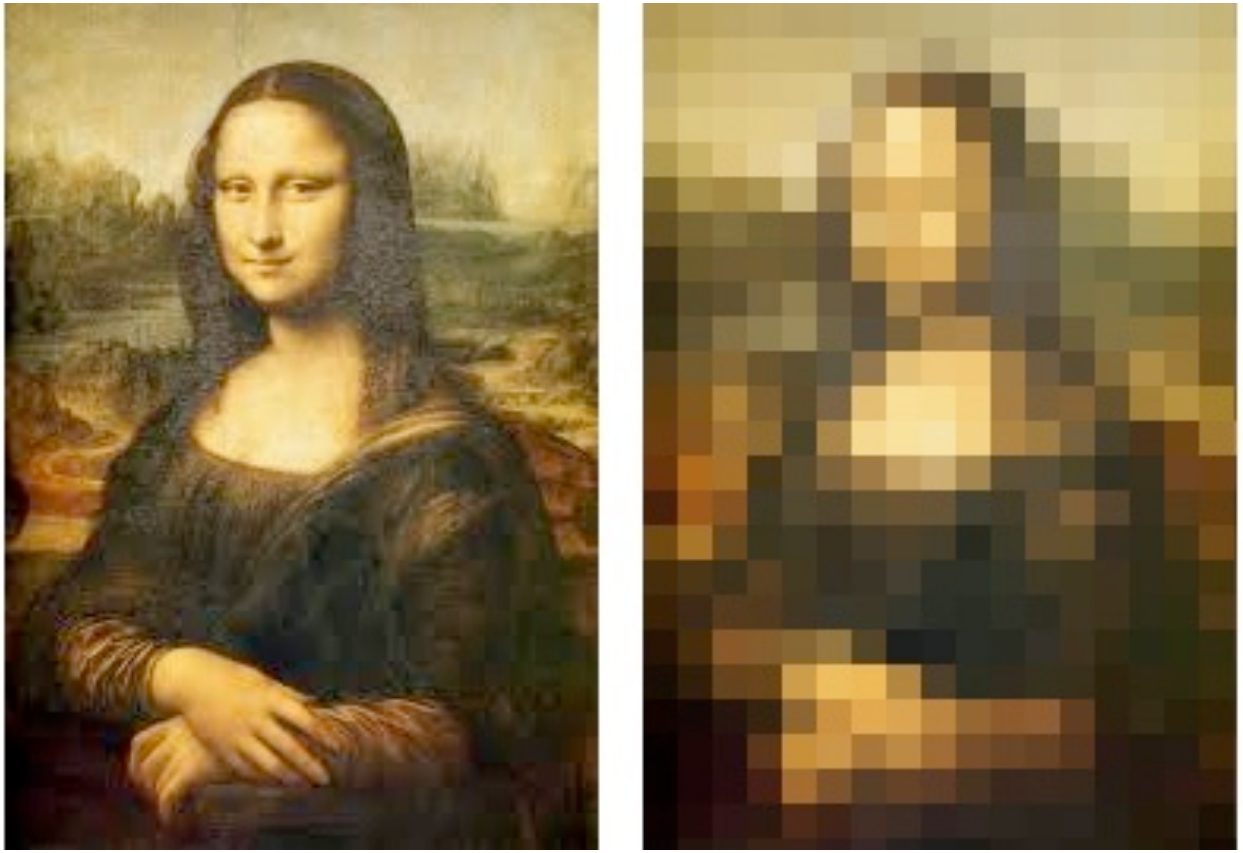

Image source: internet

From Zuhui's Earlier Talk

- **Brief introduction of CSS-OS**

CSS-OS is designed to be a survey telescope orbiting in line with the Chinese Space Station. The specifications are as follows

Project	Orbit /Site	Launch/op	FoV	R_{EE80}	Num pixels	Area	Wavelength	Num filters	spectr um
			deg^2	"	10^9	deg^2	nm		
CSS-OS 2m	LEO	~2024	1.1	0.15	2.5	17500	255—1000	7	Y
Euclid 1.2m	L2	2021	0.56 0.55	>0.2 pix lmt	0.6 0.07	15000	550—920 1000—2000	1 3	N Y
WFIRST 2.4m	L2	?	0.28	>0.2	0.3	2400	927—2000	4	Y
LSST 8.4m	Chile	2022	9.6	~0.7	3.2	18000	320—1050	6	N

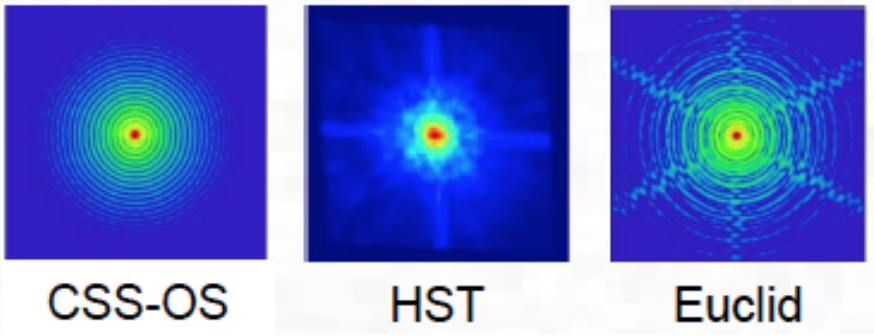

Off-axis design :
suppress the spikes

Pixelisation Effect

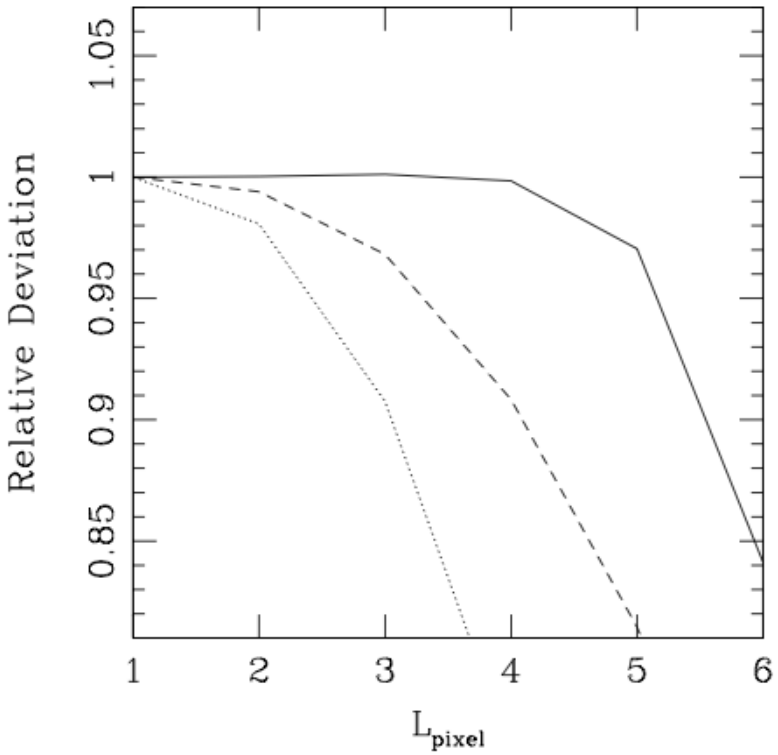

Moffat PSF

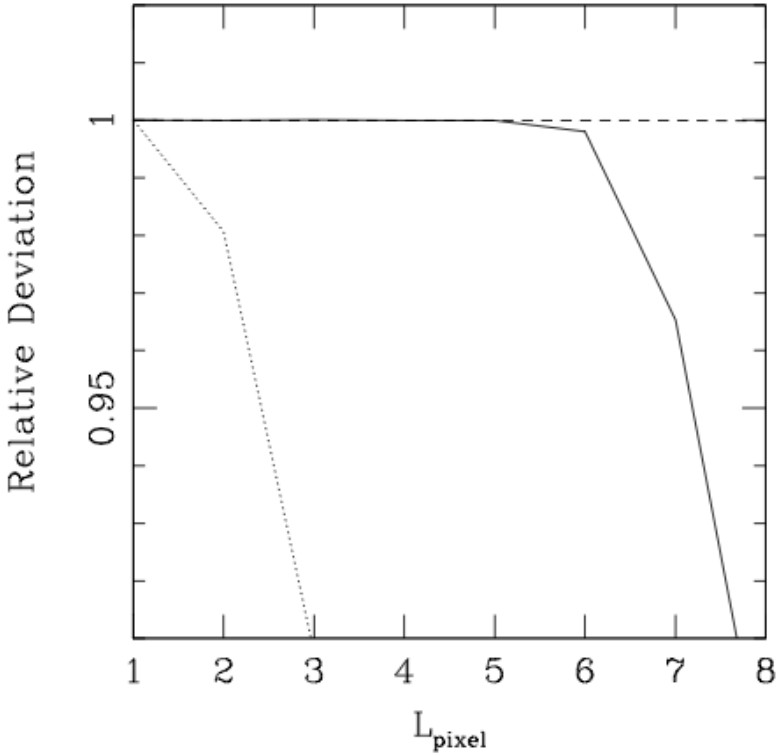

Gaussian PSF

FWHM of both PSF = 12

Pixelisation Effect

Equivalent to Whittaker－Shannon (sinc) interpolation

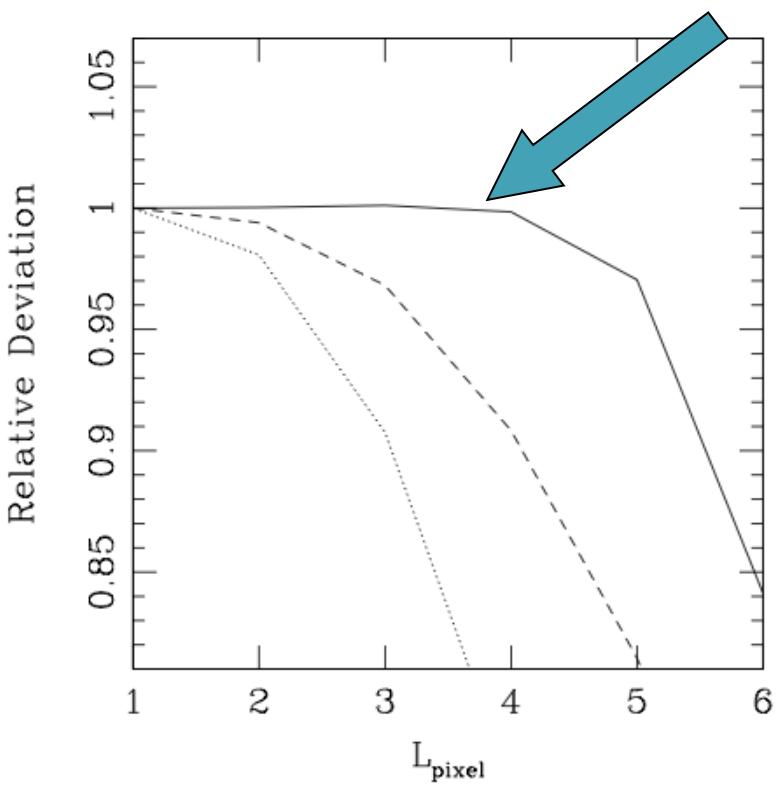

Moffat PSF

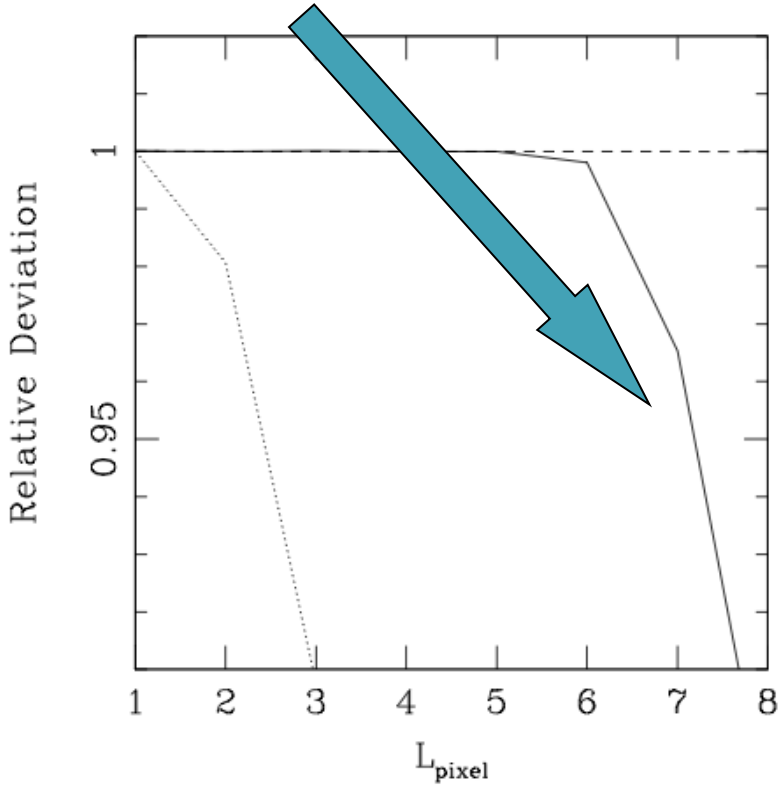

Gaussian PSF

FWHM of both PSF = 12

Dithering, MultiDrizzle

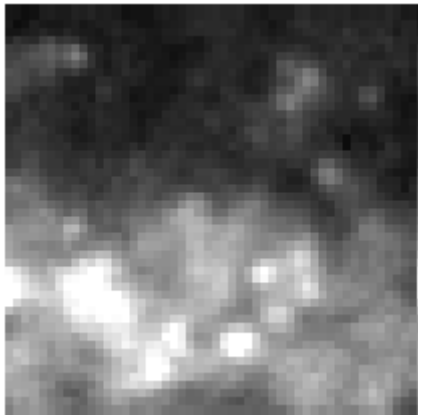

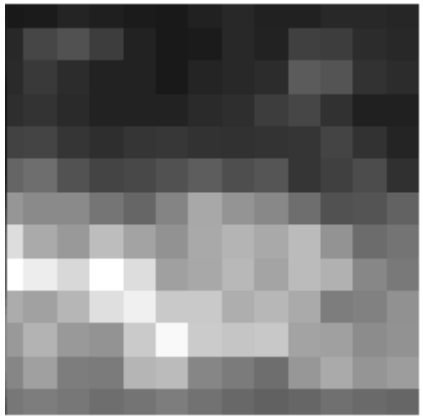

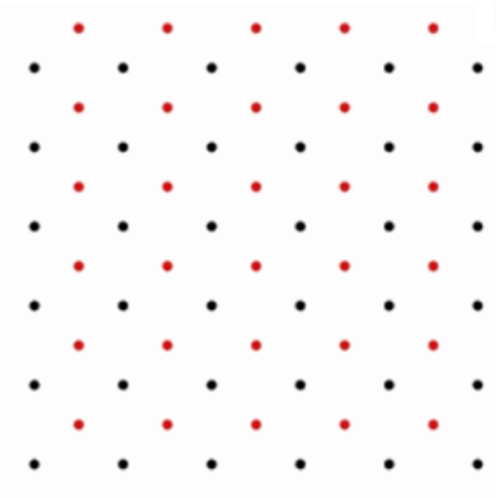

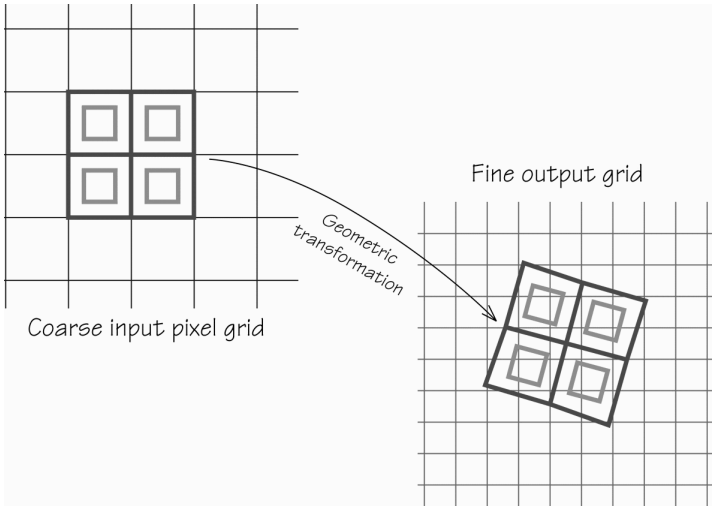

A. M. Koekemoer, A. S. Fruchter, R. Hook, W. Hack, 2002 HST Calibration Workshop, 337

Dithering: non-flat noise PS

COSMOS

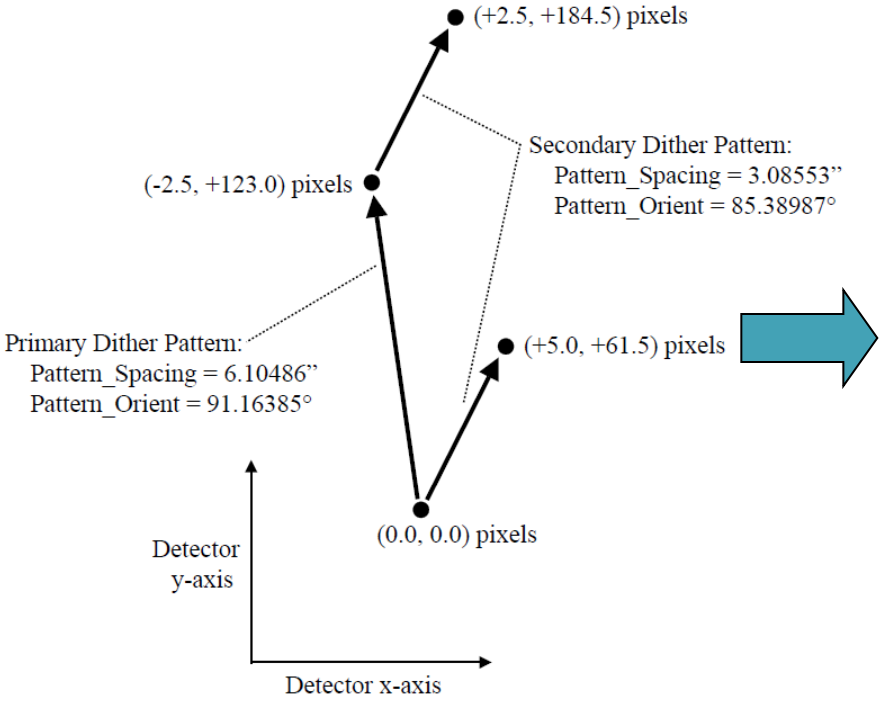

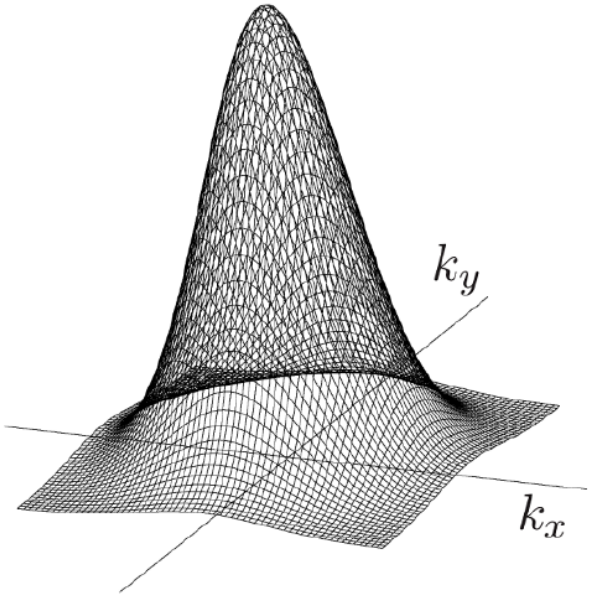

Source: Koekemoer et al. 2007

Non-flat noise power spectrum

Dithering: non-flat noise PS

COSMOS

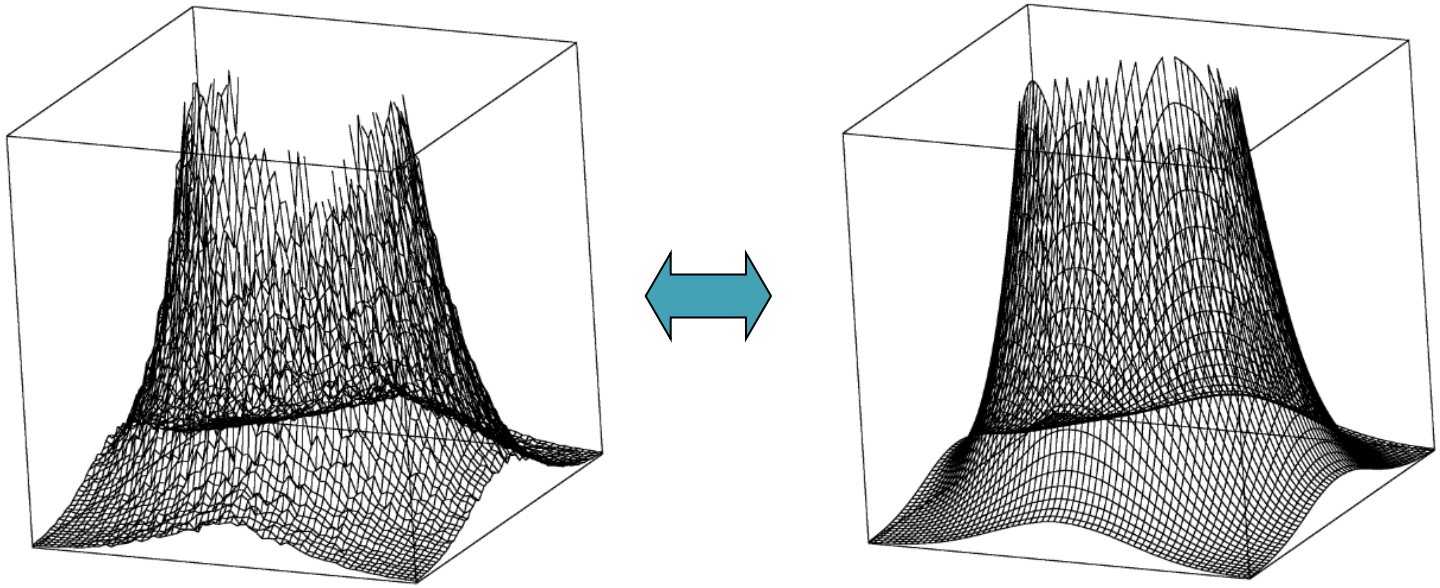

Ave of PS of sources with Mag >25

Non-flat noise power spectrum

Final Form of the Shear Estimator

$$\frac{\langle G_1 \rangle}{\langle N \rangle} = g_1, \quad \frac{\langle G_2 \rangle}{\langle N \rangle} = g_2$$

$$G_1 = -\frac{C}{2} \sum_{j=1}^{N_T} \left[(\vec{k}_j)_x^2 - (\vec{k}_j)_y^2 \right] T(\vec{k}_j) M(\vec{k}_j)$$

$$G_2 = -C \sum_{j=1}^{N_T} (\vec{k}_j)_x (\vec{k}_j)_y T(\vec{k}_j) M(\vec{k}_j)$$

$$N = C \sum_{j=1}^{N_T} \left[\left| \vec{k}_j \right|^2 - \frac{\beta^2}{2} \left| \vec{k}_j \right|^4 \right] T(\vec{k}_j) M(\vec{k}_j)$$

$$M(\vec{k}) = \left| \tilde{f}^O(\vec{k}) \right|^2 - F^O \left| \tilde{C}(\vec{k}) \right|^2 - \left| \tilde{f}^B(\vec{k}) \right|^2 + F^B \left| \tilde{C}(\vec{k}) \right|^2$$

$$F^O = \frac{\sum_{|\vec{k}_j| > k_c} \left| \tilde{f}^O(\vec{k}_j) \right|^2}{\sum_{|\vec{k}_j| > k_c} \left| \tilde{C}(\vec{k}_j) \right|^2}, \quad F^B = \frac{\sum_{|\vec{k}_j| > k_c} \left| \tilde{f}^B(\vec{k}_j) \right|^2}{\sum_{|\vec{k}_j| > k_c} \left| \tilde{C}(\vec{k}_j) \right|^2}$$

Test Result

$$g_1^{measured} = (1+m_1)g_1^{input} + c_1$$

$$g_2^{measured} = (1+m_2)g_2^{input} + c_2$$

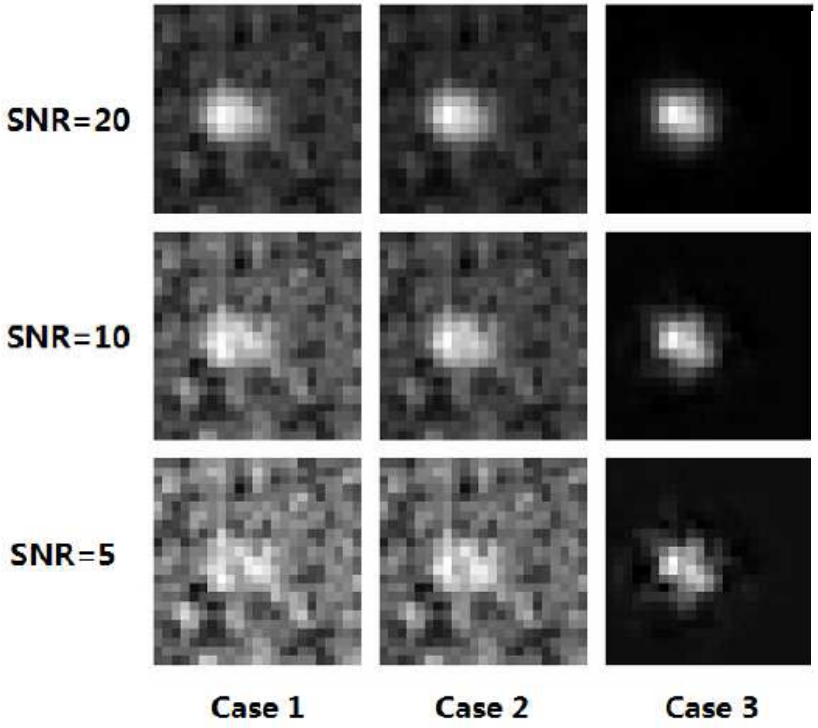

	Case 1	Case 2	Case 3
SNR= 20	$m_1(10^{-3}) : 0.9 \pm 0.1$	0.9 ± 0.08	0.9 ± 0.04
	$c_1(10^{-5}) : 0.5 \pm 0.4$	0.6 ± 0.3	0.9 ± 0.1
SNR= 10	0.8 ± 0.4	0.9 ± 0.2	0.9 ± 0.08
	0.6 ± 1.3	0.5 ± 0.7	0.8 ± 0.3
SNR= 5	0.7 ± 1.3	0.8 ± 0.7	0.8 ± 0.2
	2.1 ± 4.6	0.8 ± 2.4	0.5 ± 0.6
SNR= 20	$m_2(10^{-3}) : 1.1 \pm 0.1$	1.0 ± 0.08	1.0 ± 0.05
	$c_2(10^{-5}) : -2.9 \pm 0.4$	-2.9 ± 0.3	-2.8 ± 0.1
SNR= 10	1.3 ± 0.4	1.2 ± 0.2	0.9 ± 0.08
	-2.7 ± 1.3	-2.8 ± 0.7	-2.7 ± 0.3
SNR= 5	1.8 ± 1.3	1.5 ± 0.7	0.9 ± 0.2
	-1.9 ± 4.5	-2.6 ± 2.4	-2.6 ± 0.6

JZ, Luo, Foucaud, 2013

Pixelisation Effect

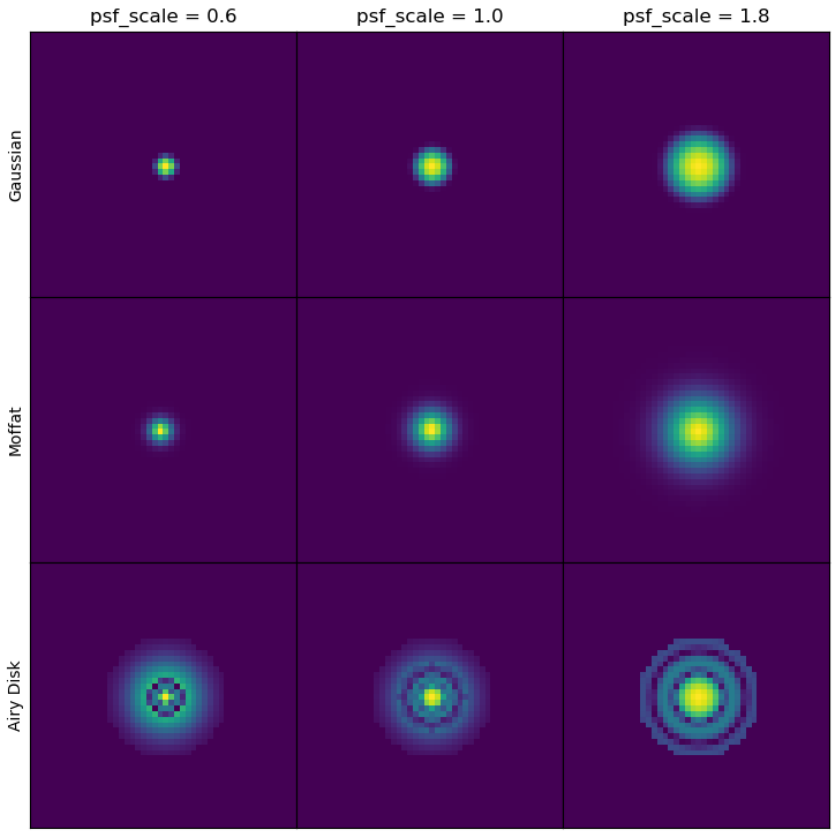

PSF Images

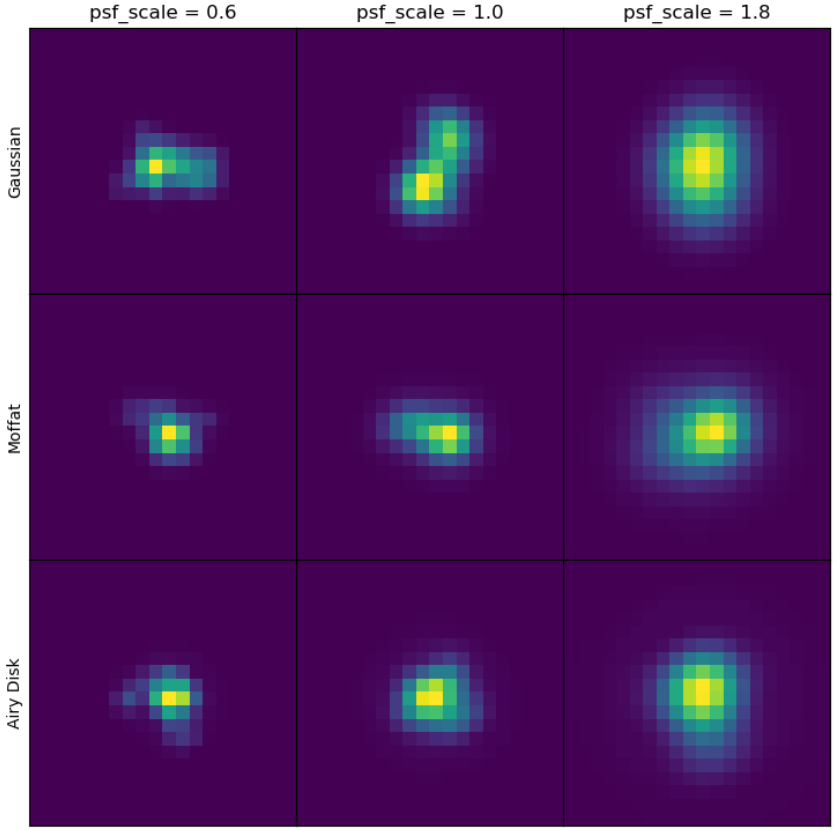

Galaxy Images

Work of Zhi Shen (沈智)

Pixelisation Effect (Some good news)

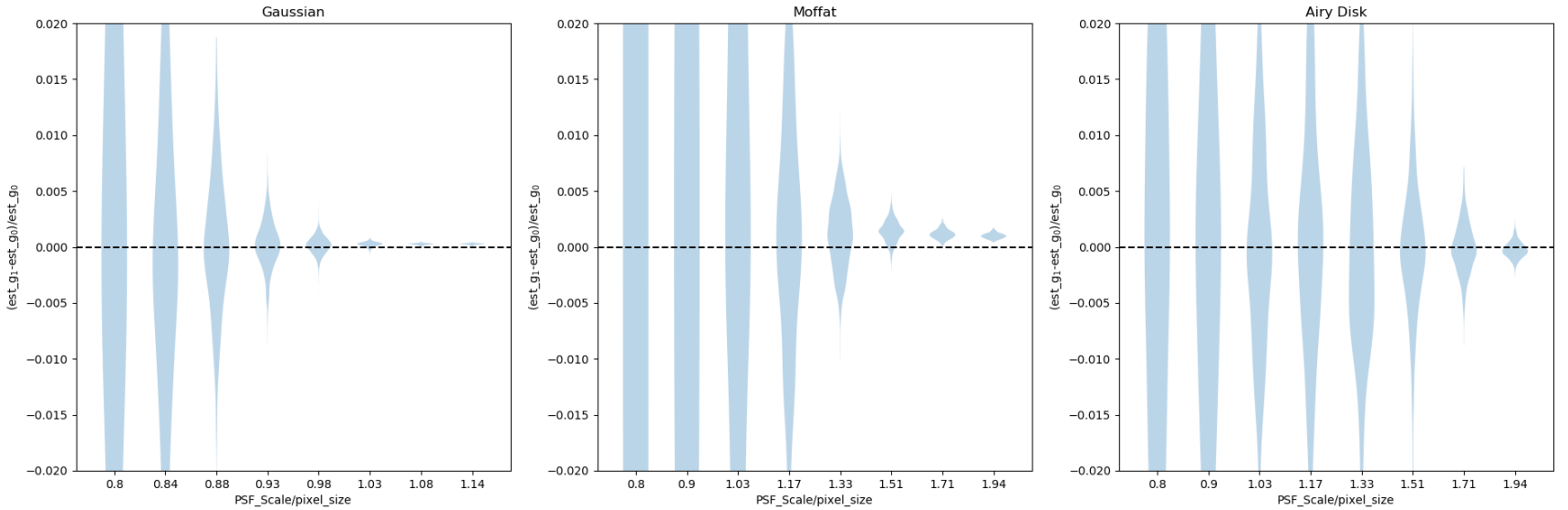

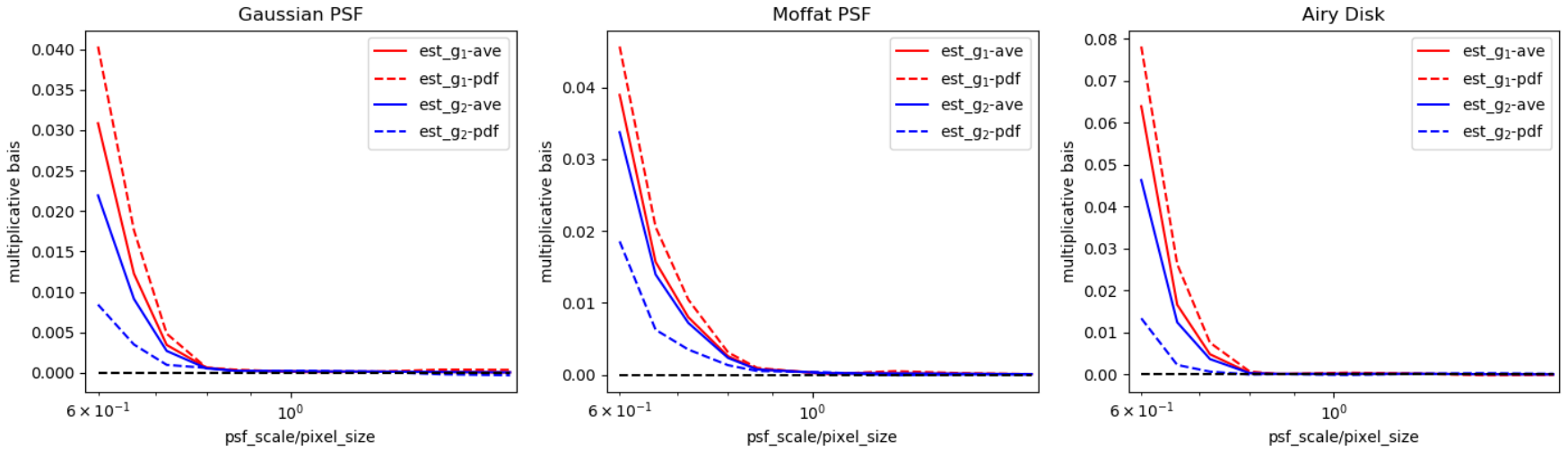

Gaussian PSF **Moffat PSF** **Airy Disk PSF**

Job Market

Department of Astronomy, Shanghai Jiao Tong University

Survey Strategy: No. of Expo per Field

CSST图像存在欠采样问题，图像信息有缺失。如何将多次曝光的图像精确组合成过采样的科学图像，并且组合后的图像在弱引力透镜的测量中不产生显著的系统误差，是一个重要的问题。目前CSST的主巡天模式对每块天区在同一波段的曝光次数是两次，如果采用传统的MultiDrizzle的方法进行图像组合，曝光次数是不够的（至少需要四次）。这里需要发展非传统的图像叠加算法。另一种可能的做法是通过模型拟合类方法测量剪切信号。这类方法的一个优点是可以容忍缺失的像素，从而可以在多张欠采样的图像上进行联合的星系模型拟合。这类方法的代表是Lensfit,目前已经被广泛应用于CFHTLenS和KiDS 等项目。无论是进行图像叠加还是利用联合的星系模型拟合，这里的关键技术问题是通过天体测量精确确定图像的方位。这个问题需要通过模拟测试。对于模型拟合类方法来说，需要研究的一个问题是实际星系形态的复杂性对测量精度可能造成的影响，以及由拟合的成功或失败对弱透镜测量造成的选择性偏差。

CCD Effects

在CCD层面，各种硬件问题或效应（Charge Transfer Inefficiency, Brighter Fatter Effect, Ghost）对图像会产生系统性的影响，对剪切信号测量造成误差。比如CTI会在CCD的信号传输方向给星系和恒星图像添加一条尾巴（由残留的电荷造成），造成图像的系统性形变。研究该效应的修正需要首先按照所选的CCD的类型和性能（比如噪声的大小），以及其性能随时间的变化，生成模拟图像，然后检验在巡天的不同时期该效应的修正可以达到的图像还原精度。在巡天的后期，由于CCD性能的下降，可以用来精确测量剪切信号的星系数密度可能减少，对于宇宙学限制的影响需要作出估计。至于Brighter Fatter Effect（起源于CCD像素内的已有电荷对于运动电荷的排斥作用）以及Ghost（起源于数据线相互影响），都需要通过模拟真实的CCD成像过程作专门的测试。

另外，在欠采样图像上，宇宙线以及其它图像缺陷的甄别也比在过采样的图像上困难。可能的做法是结合不同曝光，甚至是不同波段的曝光。

Charge transfer inefficiency due to radiation damage

All electronics gradually degrade in space, as they are bombarded with high energy radiation. This manifests itself in CCD detectors used in cameras via the generation of "charge trap" defects within the silicon lattice. During detector readout, electrons (the photoelectrons created when light falls on the detector) are temporarily captured and held in place. When these electrons are subsequently released, the rest of the image has moved closer to the readout register, so they form trails behind objects. The net effect is known as "Charge Transfer Inefficiency" (CTI). Fortunately, by modelling the process of readout and trapping, it is possible to reverse the effect, and move the electrons back to where they belong. Because the readout is the final process preformed in space, this correction should be the first analysis step performed on the ground. - Massey

Concerns (mainly about image processing)

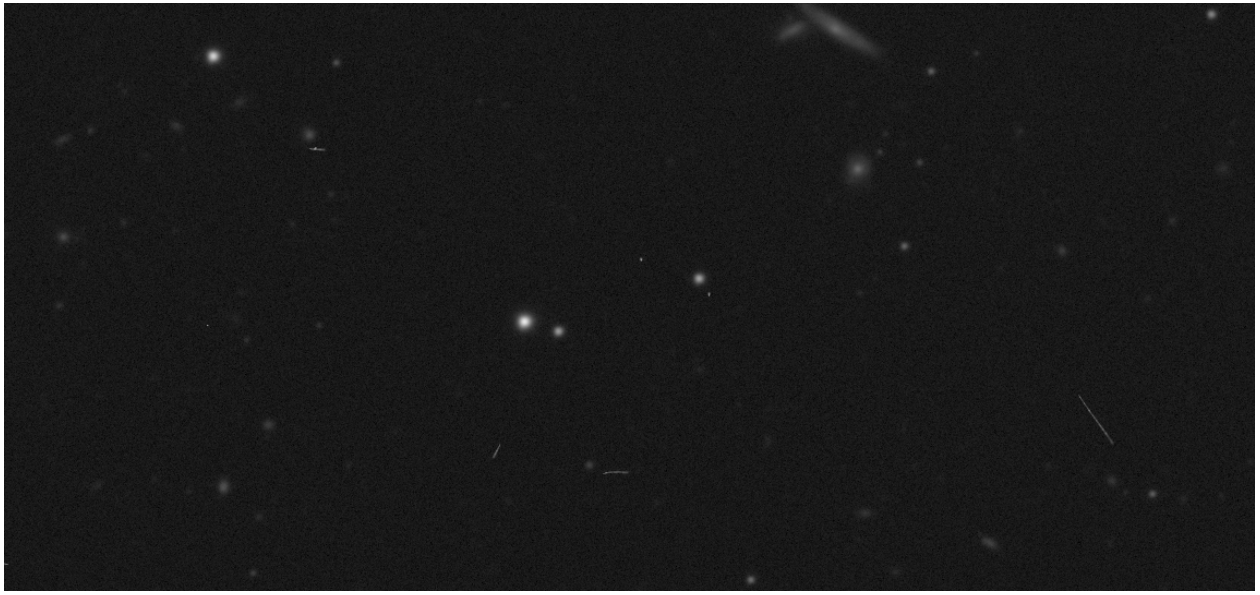

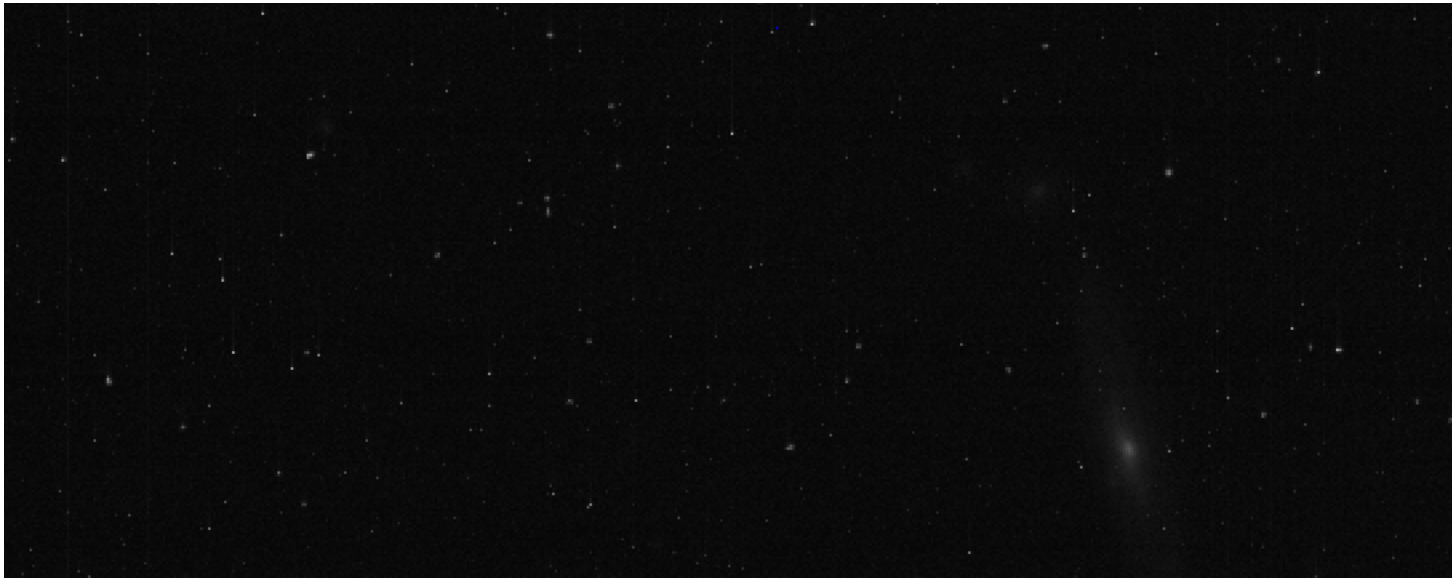

Concerns

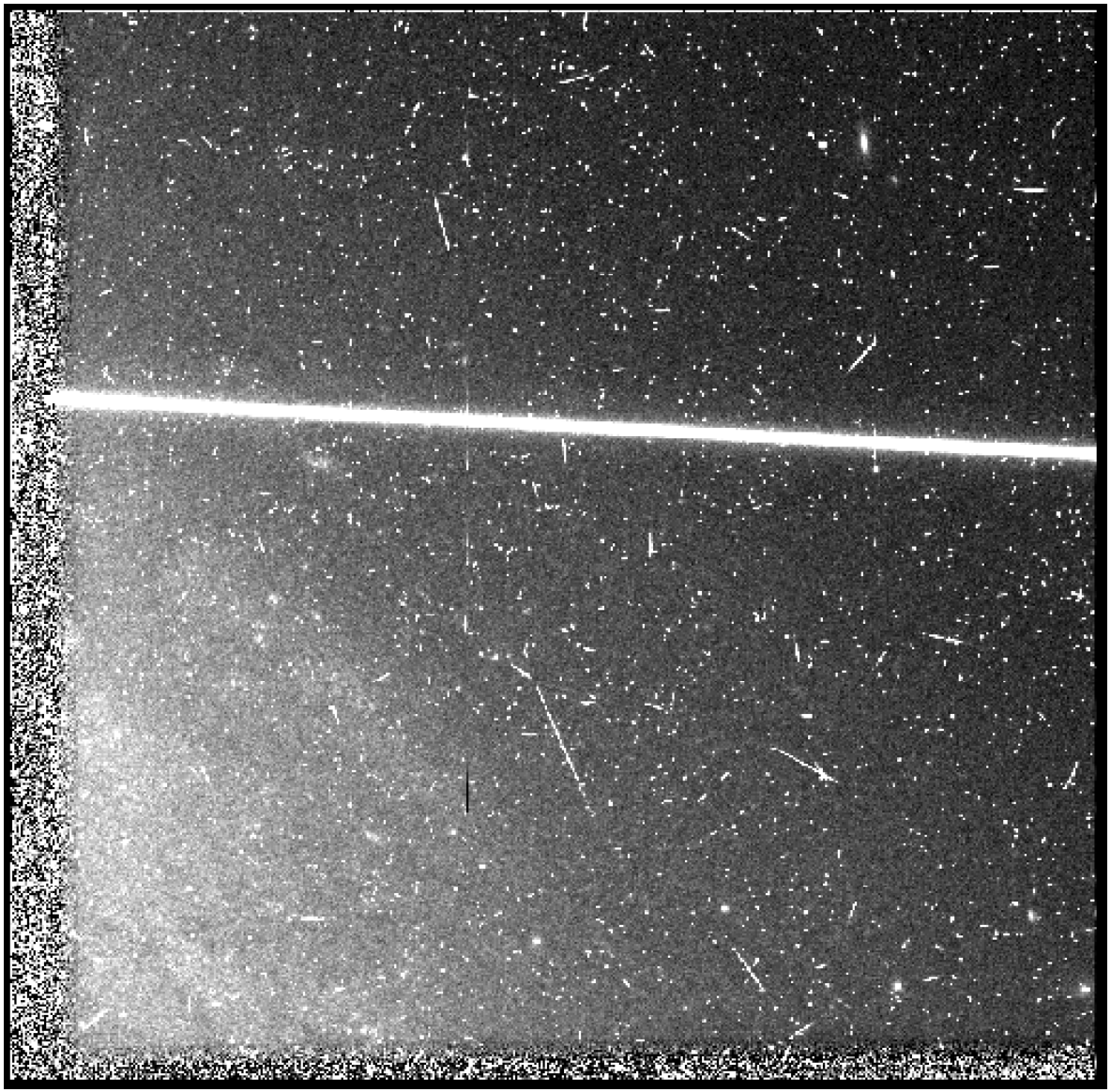

Concerns